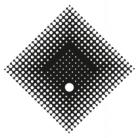
VICTORIA UNIVERSITY
MELBOURNE AUSTRALIA

A parallel volume of fluid-Lagrangian Parcel Tracking coupling procedure for diesel spray modelling

This is the Accepted version of the following publication

Yu, H, Goldsworthy, L, Ghiji, Mohammadmahdi, Brandner, PA and Garaniya, V (2017) A parallel volume of fluid-Lagrangian Parcel Tracking coupling procedure for diesel spray modelling. Computers and Fluids, 150. 46 - 65. ISSN 0045-7930

The publisher's official version can be found at
https://www.sciencedirect.com/science/article/pii/S0045793017301081
Note that access to this version may require subscription.

Downloaded from VU Research Repository https://vuir.vu.edu.au/37497/

A parallel Volume of Fluid-Lagrangian Parcel Tracking coupling procedure for diesel spray modelling

H. Yu*, L. Goldsworthy, M. Ghiji, P.A. Brandner, V. Garaniya
Australia Maritime College, University of Tasmania, Launceston, Tasmania 7250

HIGHLIGHTS

- A parallel VOF-LES/LPT-LES coupling procedure for complete spray simulation.
- Characteristics of the in-nozzle flow phenomena.
- Analysis of primary and secondary diesel atomisation.

Abstract

A parallel Eulerian/Lagrangian multi-scale coupling procedure for diesel spray simulation is presented. Early breakup of the diesel jet together with in-nozzle flow separation and turbulence are captured by employing a compressible Volume of Fluid (VOF) method integrated with LES turbulence modelling and a basic cavitation model. In regions where the phase interface can no longer be sufficiently resolved, separated and small scale liquid structures are described by a Lagrangian Parcel Tracking (LPT) approach, in conjunction with secondary breakup modelling and the implementation of an LES stochastic dispersion model. The coupling of these two descriptions utilises a Region Coupling Method and an efficiently parallelised droplet identification and extraction algorithm. This approach enables run-time VOF-LPT field coupling and filters small-scale liquid structures that are suitable candidates for Eulerian-liquid-structure/Lagrangian droplet conversion, preserving their position, mass and

*Corresponding author.
Email address: hongjiang.yu@utas.edu.au (H. Yu)

momentum. The simulation of a diesel spray from a nozzle with a sharp entrance shows the capability of the coupling procedure as a feasible tool for the prediction of complex spray dynamics.

Keywords: Volume of Fluid, Lagrangian Parcel Tracking, Large Eddy Simulation, Parallel Region Coupling, In-nozzle flow, Primary and Secondary Atomization.

---

1. Introduction

Achieving an efficient combustion process in diesel engines requires optimally combined effects of air and fuel mixing, turbulence generation and interaction of spray and engine geometry. This involves improving the atomisation of the diesel spray by taking into account various operating conditions such as different nozzle designs, operation temperatures as well as the injection and chamber pressures. Many studies have focused on these aspects in an effort to realise more efficient combustion and reduced emissions [1].

In diesel engines, the fuel is injected at a high pressure into the combustion chamber where it undertakes a series of disintegration processes. Initially, the interaction between the fuel and nozzle geometry results in a flow regime dominated by separation, cavitation and aerodynamic instabilities causing primary jet break-up in the vicinity of the nozzle exit [1, 2]. In this process, the fragmentation of the intact liquid core generates large liquid structures that will undergo secondary breakup and further

disintegrate into small droplets. At the next stage, the spacing between droplets increases further downstream of the nozzle due to the turbulent droplet-gas interaction and the droplet size decreases owing to the secondary breakup regime.

The primary and secondary breakup mechanisms have been extensively studied experimentally, see for example [3-8]. The use of different measuring techniques especially X-ray analysis of diesel sprays has provided comprehensive information on the liquid penetration, cross-sectional projected density distribution and the Sauter Mean Diameter (SMD). The measurement of these parameters can help gain a qualitative understanding about the diesel spray evolution. However, the shot to shot variation of sprays makes it difficult to quantitatively capture the detailed features of the spray at different stages [4]. Therefore, to obtain information on the spatial and temporal spray evolution with high resolution, performing computational simulations is essential.

Due to the complex behaviour of the diesel spray in the primary and secondary atomisation processes, various computational approaches have been proposed and developed to simulate these processes. For the primary atomisation, interface capturing/tracking methods such as the Volume of Fluid (VOF) method [9-12], Level Set Method [13, 14] and the combination of both[15, 16] are widely adopted. In the VOF method, the liquid and gas are treated as two immiscible phases that are both described in the Eulerian framework. A transport equation calculating the volume

fraction of each phase in a cell is employed and the derived gradient of the volume fraction of the dense phase is used to construct the liquid interface. This intrinsically allows the simulation of jet breakup, liquid core disintegration and droplet coalescence in a volume conservative manner. However, at least 5 cells are required for sufficiently describing an individual liquid structure, leading to excessive demand in mesh density and computational time for complex two-phase flow cases. In the secondary atomisation, due to the increasingly dominant effect of surface tension on small scales, small liquid structures start to become either spherical or elliptical, and they fall in the framework of LPT. However, in order for these small structures to be valid for Lagrangian modelling, they need to be at least five times smaller than the grid size. This is one of the main limitations of the Lagrangian modelling that grid size could be larger than might be desirable for good resolution of small scale flow features. A wide range of Lagrangian models have been developed specifically for the modelling of spray atomisation. Most of these are based on the Lagrangian description of individual droplets or parcels with an additional level of modelling for the primary and secondary atomisation [17-25]. The comparison of four different atomisation models, namely the Blob model [26], the Huh and Gosman atomisation model [27] and the MPI-1 and MPI-2 atomisation models is detailed in [28]. One of the drawbacks of these models is the lack of detailed attention to the effects of in nozzle flow phenomena (e.g. flow separation, cavitation and turbulence), resulting in the inaccurate prediction of primary spray breakup. However, they possess the advantage that it is rather efficient

to simulate the evolution of a cluster of small-scale liquid structures without a high demand in computational time. This is enabled by the use of many well-developed secondary breakup models. Typically, the wave model by Reitz [19] as one of the earliest developed droplet breakup models predicts the development of aerodynamically induced disturbances on the liquid surface employing the Kelvin-Helmholtz (KH) mechanism. This mechanism relates the radii of parent and child parcels with the fastest growing wave length on the liquid surface and its corresponding growth rate. The RT model by Amsden *et al.* [29], on the other hand, describes Rayleigh-Taylor instabilities growing on a liquid-gas interface due to the density jump between gas and liquid. A parameter known as the break up time is introduced in this model, and it acts as a trigger to initiate the breakup process when the growing time of RT waves on the droplet surface is greater than the break up time. A hybrid model combining the KH and RT models is then developed to account for both the primary and secondary break up of jets using a switching threshold Weber Number We = 12 [30].

Recently, Large Eddy Simulation (LES) has been extensively integrated with interface tracking/capturing and Lagrangian Parcel Tracking (LPT) methods. Particularly, several sub-grid surface tension LES models have been proposed and demonstrated to be valid in [31-33], especially for the prediction of in-nozzle flow and the ensuing primary atomisation. They are based on either LSM or VOF with sharp interface reconstruction algorithms. Despite being highly accurate, the additional modelling for

interface reconstruction and sub-grid surface tension imposes computational constraints limiting their application to simple and small two-phase flow cases. LES has also been demonstrated to provide good spray behaviour prediction with Lagrangian methods in [17, 25, 34, 35]. In particular, the interaction between the droplets and the surrounding gases at sub-grid level is studied by Jangi *et al.* [22] from which it was concluded that the dispersion of spray droplets due to sub-grid fluid kinetic energy has a significant effect on the evolution of the entire spray.

In the light of the development of various primary and secondary atomisation modelling approaches, many successful attempts have been made to combine the merits of interface tracking/capturing and Lagrangian particle tracking. One of the first Interface-Tracking/Point Particle Tracking coupling algorithms for jet breakup simulation is reported by Hermann *et al.* [36]. A dual grid method in which Eulerian (Level Set) and Lagrangian (point particle tracking) descriptions of liquid spray are handled respectively on two individual grids with two-way momentum coupling was first introduced in spray modelling. A similar approach however with adaptive mesh refinement capability is demonstrated by Tomar *et al.* [37] where the liquid interface is captured by using a local mesh refinement algorithm and small droplets are tracked as Lagrangian spherical particles in the region where the mesh is sufficiently coarse. Both approaches identify liquid structures having a volume smaller than a predefined threshold value from the Eulerian simulation and transfer them into individual

particles eligible for particle tracking. These methods are often referred to as the Direct Coupling Approach (DCA) and provide unique ways to deal with mesh inconsistency problems encountered in simultaneous modelling of primary and secondary spray atomisation. One of the main drawbacks of DCA is the limitation that droplets generated from Eulerian simulation can only be expensively tracked as individual particles due to the absence of secondary breakup modelling. This is either because the exclusive use of velocity field information in the Eulerian-Lagrangian coupling disables the use of a secondary breakup model [36] or the computational power cannot afford the integration of an adaptive mesh refinement method with secondary breakup modelling [37]. The secondary breakup models, typically the KH-RT model, can group fluid particles of similar properties in a limited number of parcels. The use of the parcel concept can ease the computational strain by reducing the number of individual particles tracked in the Lagrangian modelling of the spray. Without the parcel assumption, the application of the DCA methods to detailed study of complex multiphase flow is computationally restricted. Alternatively, the development and implementation of a Eulerian-Lagrangian Spray Atomisation (ELSA) model attributed to Vallet *et al.* [38] and Desportes *et al.* [39] effectively integrated the Lagrangian parcel tracking with a single phase Eulerian model. However, this model treats liquid and gas as a single phase mixture, hence the surface tension effect is not accounted for. The evaluation of mean size of the liquid ligaments is determined only by solving a transport equation for liquid/gas interface density. More recent developments in spray

modelling give rise to many mathematical approximations that statistically couple the primary and secondary atomisation processes. One representative study conducted by Grosshans *et al.* [40] presents the use of a coupling layer located within the region where the transition from primary to secondary atomisation occurs. The volume, velocity and position of liquid structures are sampled on the coupling layer in the Eulerian frame work till statistical convergence is achieved. Sampled data are then implemented as initial conditions with the parcel assumption for the subsequent modelling of secondary atomisation in a Lagrangian reference. In contrast, the probability density functions of the droplet size were extracted from the entire Eulerian domain by Befrui *et al.* [41] and the sampled size distribution data were used to reinitialise the spray simulation using the Lagrangian parcel tracking method. The statistical coupling procedures are advantageous in terms of efficiency and have relatively higher accuracy as compared to the pure Lagrangian description of the liquid spray. However, the stochastic way in which data are sampled and initialized for the second stage of spray modelling inevitably compromises the flow information supplied by the more accurate Eulerian modelling of the in-nozzle flow, which needs to be approached using more advanced modelling methods.

The objective of this study is therefore to advance the recent work [11, 36, 40, 41] using an open source finite volume tool Open-Foam by (1) development of a parallel processing algorithm for the identification and extraction of droplets from VOF-LES

simulation and injecting them in the LPT-LES framework, (2) integration of a sub-grid stochastic turbulent droplet dispersion model to improve the capability of an existing Lagrangian solver in OpenFoam, (3) development of a conservative region coupling procedure that allows runtime exchange of fluid information between VOF-LES and LPT-LES in the region where Eulerian-Lagrangian transition occurs and (4) allow the modelling of the secondary breakup of large droplets extracted from the VOF-LES and the generation and tracking of child parcels in the LPT-LES simulation.

The advanced capabilities of the developed code enable simulation of the complete evolution of the diesel spray from in-nozzle flow to the atomised droplets. This study demonstrates that the runtime region coupling of VOF-LES and LPT-LES is a feasible tool-chain for the prediction of spray atomisation processes.

2. Numerical Methods

2.1. Region Coupling Method

One of the most challenging problems in diesel spray simulation is the different scales with which the continuous phase and the dispersed phase are modelled. Specifically, the primary breakup of liquid jets requires a refined grid system to capture the surface instabilities which generate large ligaments. These ligaments further interact with surrounding gases to produce smaller liquid structures (droplets) which are rather expensive to be discretised by an even finer grid. They fall in the Lagrangian reference that entails a coarse grid typically 5 times the size of droplets to satisfy the

Lagrangian approximation. This mesh inconsistency problem has been tackled either by a dual grid approach [11, 36] or a statistical coupling [40, 41] with the former being more accurate and the latter being more computationally efficient. The dual grid approach uses two entirely overlapping grids of different resolution, between which the exchange of momentum is through a conservative interpolation scheme [14]. However, due to the discrepancy in resolution between the two grids, the loss of background flow information is inevitable in the interpolation process. This problem is more severe in most statistical coupling approaches, which utilise statistically converged data sampled from the Eulerian simulation to initialise the Lagrangian simulation. The Region Coupling Method (RCM) described in this section overcomes the problems of both approaches.

The RCM employs two grids that are only partially overlapping. The overlapping region is where the transition from primary to secondary spray atomisation occurs and it couples the VOF and LPT simulations with two identical overlapping grids. To put it into perspective, Figure 1 shows the position of this region in relation to the spray. The spray development is divided into three stages, namely the primary breakup stage when an intact liquid core is present, the transition stage (dense region) at which the liquid core starts to disintegrate into large ligaments and finally the diluted phase in which small liquid structures form and are dispersed by the carrier phase.

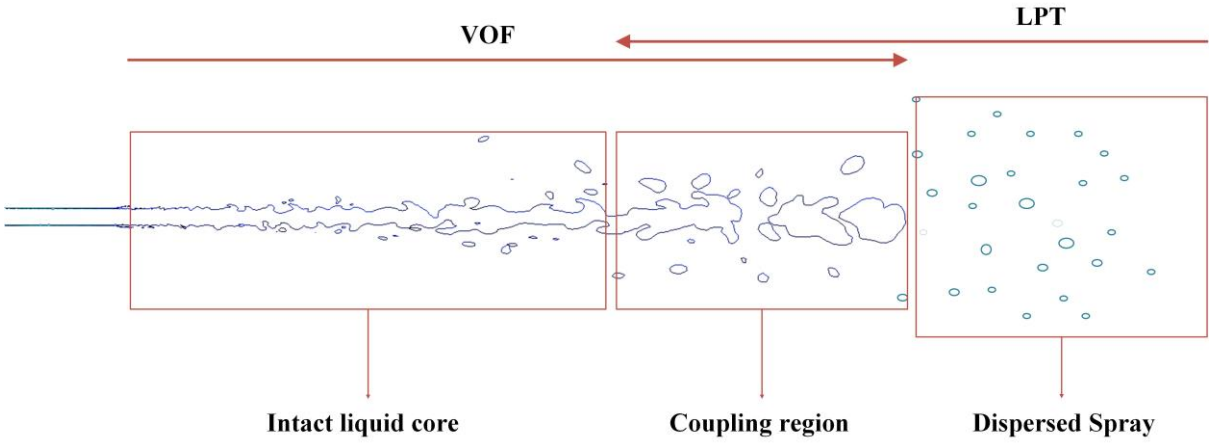

Figure 1: Region VOF-LPT coupling for a liquid diesel spray. The RCM is employed in the coupling region where VOF and LPT overlaps.

One disadvantage of the RCM is that a decision has to be made as to where to place the overlap region, which requires that the Eulerian code needs to first be run till the liquid penetration reaches maximum. However, a relatively coarse mesh can be employed with the VOF method to estimate the maximum liquid penetration. Alternatively, the use of generic experimental data can also help determine the extent of a diesel spray by using the Musculus and Kattke model [42, 43]. The present study utilises an incremental method where the VOF domain was gradually extended to accommodate the maximum liquid penetration. This is achieved through expanding the VOF computational domain incrementally along the penetration and reinitialising the simulation with the new domain by mapping the field data from the previous simulation. After the maximum liquid penetration has been estimated, the coupling region should be placed to encompass the entire dense region that most large ligaments reside in.

In the coupling region, it is computationally difficult to sufficiently describe all liquid structures of different scales using a refined grid with the VOF method. Therefore, the mesh resolution is progressively coarsened along the penetration of the liquid jet. The transition from a fine grid to a relatively coarse grid corresponds to the transition from VOF to LPT. The transition from VOF to LPT results in the decrease in the number of mesh elements that can be used to capture the interface of a liquid structure. At some points, the generated liquid structures can become smaller than 5 mesh cells combined and their liquid surfaces can no longer be captured by the VOF method. These liquid structures are identified and converted to Lagrangian droplets if their volumes are smaller than those of the local cells in which their centroids lie. Therefore, a Droplet Identification Algorithm (DIA) and a Droplet Extraction Algorithm (DEA) comparing the volume of a liquid structure with the volume of a local cell containing this structure's centroid are developed. The code automatically adapts to the grid and frees users from defining a fixed threshold volume. It allows a greater variety of droplet diameters with a non-uniform grid than a uniform one. However, a threshold percentage determining the amount by which a liquid structure is smaller than its host cell needs to be defined. In this study, a liquid structure is recognised as a suitable Lagrangian droplet candidate if it has a volume smaller than 20% of the host cell's volume in the coupling region. The process is illustrated in Figure 2.

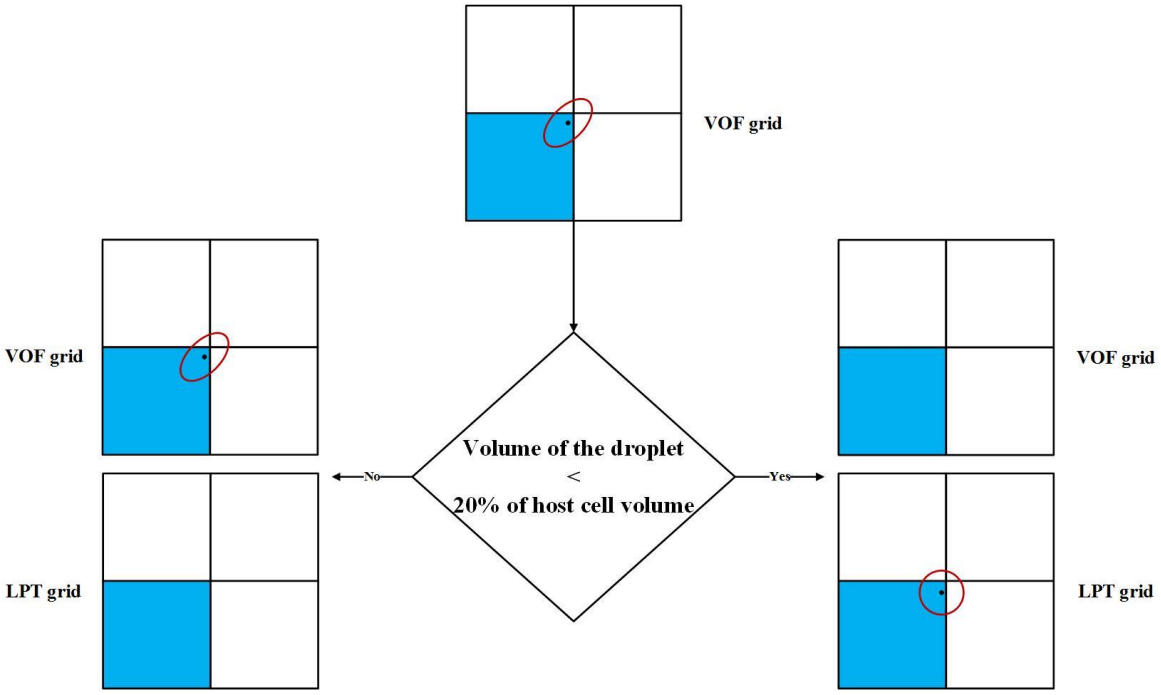

Figure 2: Process diagram for the treatment of a droplet that is smaller than its host cell. The droplet is represented by a red ellipse with its centroid residing in the host cell shaded in blue. The converted spherical Lagrangian droplet is inserted at the same position in the shaded cell of the LPT domain.

The droplet conversion procedure enables the use of identical grids for both the VOF and LPT simulations in the coupling region. It solves the mesh inconsistency problem and allows high fidelity field coupling between VOF and LPT as the field mapping can be performed between two identical grids.

To reduce the computational intensity, the DIA and DEA as well as the two-way field mapping between VOF-LES and LPT-LES are deployed only in the coupling region. The two-way field mapping uses a volume conservative coupling algorithm taken from the parallel map-Fields utility of Open-Foam [44], known as cellVolumeWeight. It is a volume averaging algorithm that allows conservative mapping of vector and scalar fields between two grids.

2.2. VOF-LES

The VOF-LES employed in the present study is based on a mathematical model composed of governing equations for the conservation of mass and momentum of a two-phase system, accredited to E. De Villiers *et al.* [45]. This system comprises two immiscible, compressible fluids and accounts for the surface tension between the two-phases. The single set of mass and momentum transport equations are

$$\frac{\partial \rho}{\partial t} + \nabla \cdot (\rho U) = 0 \tag{1}$$

$$\frac{\partial \rho U}{\partial t} + \nabla \cdot (\rho U \otimes U) = -\nabla P + \nabla \cdot \tau + \int_{S(t)} \sigma \kappa n \cdot \delta(x - x^{'}) ds \tag{2}$$

where U is the velocity and ρ is the mixture density. The mixture density ρ is closely related to the local volume fraction α of each phase with $\alpha = 1$ representing a computational cell fully filled with liquid, while $\alpha = 0$ indicates a cell entirely occupied by gas. Any cell having $0 < \alpha < 1$ contains an interface segregating liquid and gas. For liquid-gas calculations, the mixture density in each computational unit is obtained from

$$\rho = \alpha_l \rho_l + (1 - \alpha_l) \rho_g \tag{3}$$

where α_l is the volume fraction of liquid phase, ρ_l and ρ_g are the respective liquid and gas densities.

The integral term in equation (2) is a Dirac function that only produces a non-zero value when $X = X^{'}$ which is an indication of the existence of a liquid interface. This

source term accounts for the effect of surface tension force on the liquid jet breakup process. The evaluation of this term is achieved following E. De Villiers *et al.* [45] through the continuum surface force model of Brackbill *et al.* [46] as

$$\int_{S(t)} \sigma n\kappa \cdot \delta(x - x')ds \approx \sigma\kappa\nabla\alpha \tag{4}$$

where σ is the surface tension coefficient, α is the volume fraction of the liquid phase which is obtained from the solution of a transport equation

$$\frac{\partial \rho\alpha}{\partial t} + \nabla \cdot (\rho U\alpha) = 0 \tag{5}$$

and n is a unit vector normal to the liquid surface, κ is the interface curvature calculated from the solution of liquid phase volume fraction α

$$\kappa = \nabla \cdot \left(\frac{\nabla\alpha}{|\nabla\alpha|} \right) \tag{6}$$

The system of equations is closed by an equation of state

$$\begin{cases} \rho_l = p\psi_l \\ \rho_g = p\psi_g \end{cases} \tag{7}$$

with ψ_l and ψ_g being the compressibility for liquid and gas phases respectively. The dynamic viscosity of the mixture is obtained through

$$\mu = \alpha_l\mu_l + (1 - \alpha_l)\mu_g \tag{8}$$

The VOF interface tracking method is a simple and flexible approach for the prediction of multi-phase flows. A major limitation of this method is its limited ability to preserve sharp interfaces without an interface reconstruction algorithm such as

Piecewise Linear Interface Construction (PLIC) [47]. High resolution prediction of flow with a free liquid surface is often achieved by local (Adaptive Mesh Refinement [37]) or global grid refinement [48]. The present study adopts a globally refined grid for the VOF simulation. Another limitation of the current compressible VOF method is that the generated gas at low pressure sites is given the properties of air due to the lack of a phase change model. This gas does not condense back to liquid fuel when the local pressure recovers to above the vapour pressure. This can be referred to as a basic cavitation model but without the modelling of phase change.

The LES model is integrated in equations (1), (2) and (4) through a local volume averaging procedure that decomposes relevant phase-weighted hydrodynamic variables into resolvable and sub-grid scale components. The elimination of the sub-grid fluctuations from direct simulation is done through a filtering process together with the non-linear convective terms in equation (2). This process generates additional terms comprising correlation of sub-scale variables that entail closure through additional modelling. Of these terms, the most crucial one is the Sub-Grid-Scale (SGS) stress that governs the effect of unresolved turbulence scales on momentum transport process and its dissipation. This term is defined as

$$\tau_{sgs} = \overline{UU} - \overline{U}\,\overline{U} \tag{9}$$

The closure of the SGS stress is achieved through a sub-grid eddy viscosity model given as

$$\tau_{sgs} + \frac{\mu_{sgs}}{\rho}(\nabla\overline{U} + \nabla\overline{U}^{T}) = \frac{2}{3}kI \tag{10}$$

in which k is the SGS turbulence kinetic energy and μ_{sgs} is the SGS turbulent viscosity. These SGS turbulence parameters are calculated by using a one-Equation eddy model for evaluating k attributed to Yoshizawa [49].

$$\frac{\partial \rho k}{\partial t} + \nabla\cdot(\rho k\overline{U}) - \nabla\cdot\left[(\upsilon + \upsilon_{sgs})\nabla k\right] = -\frac{1}{2}\tau_{sgs} : (\nabla\overline{U} + \nabla\overline{U}^{T}) - \varepsilon \tag{11}$$

where $\varepsilon = C_{\varepsilon}\rho k^{(3/2)} / \Delta$ is the turbulent dissipation, $\upsilon_{sgs} = C_k k^{(1/2)}\Delta$ is the SGS kinematic viscosity ($\Delta = \sqrt[3]{V}$ represents the SGS length scale in which V represents the volume of the computational cell under consideration). The turbulent coefficients found from statistical analyses are $C_k = 0.07$ and $C_{\varepsilon} = 1.05$ [49]. As the emphasis of this study is placed mainly on obtaining reasonable resolution of spray simulation and the current implementation of LES is sufficient for this purpose, other SGS terms pertaining to density, mass transfer, phase fraction and surface tension are neglected.

2.3. LPT-LES

The LPT-LES method is derived based on the consideration of momentum exchange between the gas phase and the dispersed liquid phase, which is primarily described in the work of Jangi *et al [22]*. This is done through including additional source terms for the exchange rate of mass ($S_{\rho}^{s} = S_{Z}^{s}$), momentum (S_{U}^{s}) and heat (S_{h}^{s}) between the two phases in the gas phase governing equations, while the dynamics of the liquid phase are handled by Newton's second law. The evaporation of fuel is not considered in the

present study as the spray is modelled at room temperature, therefore S_{ρ}^{s} and S_{Z}^{s} are assumed to be zero. The Favre-filtered LES conservation equations for the gas phase can be expressed as

$$\frac{\partial \overline{\rho}}{\partial t} + \nabla \cdot (\rho U) = \overline{S_{\rho}^{s}} = 0 \tag{12}$$

$$\frac{\partial \overline{\rho} U}{\partial t} + \nabla \cdot \left[\overline{\rho} UU - \overline{\tau} + \tau_{sgs} \right] = \overline{S_{U}^{s}} \tag{13}$$

$$\frac{\partial \overline{\rho} h}{\partial t} + \nabla \cdot (\overline{\rho} U h) - \nabla \cdot \left[\overline{\lambda} \nabla \cdot T + h_{sgs} \right] = \overline{S_{h}^{s}} \tag{14}$$

$$\frac{\partial \overline{\rho} Z}{\partial t} + \nabla \cdot (\overline{\rho} U Z) - \nabla \cdot \left[\overline{\rho D} \nabla \cdot Z + \Phi^{Z}{}_{sgs} \right] = \overline{S_{Z}^{s}} = 0 \tag{15}$$

The over-line signifies the general filtering

$$\overline{\phi(x,t)} = \int G(r,x) \phi(x - r, t) dr \tag{16}$$

where the integration is applied to the entire field with the filtering function satisfying the normalization condition

$$\int G(r,x) dr = 1 \tag{17}$$

The tilde represents the Favre filtering

$$\overline{\rho \phi} = \overline{\rho} \widetilde{\phi} \tag{18}$$

in which ϕ is a dependant fluid field variable.

Apart from general fluid parameters, enthalpy h, thermal diffusion coefficient λ, mass diffusion coefficient D, mixture fraction Z and SGS species mass fluxes $\Phi^{Z}{}_{sgs}$ can be introduced to account for energy exchange and to ensure conservation. While the one-equation eddy model can be utilised to estimate the SGS stress term τ_{sgs}, the

additional terms h_{sgs} and Φ^{Z}_{sgs} entail closure in order to close equations (13)-(16). They are modelled using a gradient diffusion-closure

$$h_{sgs} = -\overline{\rho C_p} \frac{\upsilon_{sgs}}{\mathrm{Pr}^{sgs}} \nabla \cdot T \tag{19}$$

$$\Phi^{Z}_{sgs} = -\rho \frac{\upsilon^{sgs}}{Sc^{sgs}} \nabla \cdot Z \tag{20}$$

In Lagrangian spray simulation, the spray is considered as a discrete phase comprising a large quantity of parcels that are transported using Newtown's second law. The LPT method then provides closure for the source terms $\overline{S_U^s}$ in equations (14). The dynamics equations of the dispersed liquid phase are expressed as

$$\frac{d}{dt} X_P = U_P \tag{21}$$

$$\frac{d}{dt} U_P = \frac{C_D}{\tau_P} \frac{\mathrm{Re}_P}{24} (U_g - U_P) = \frac{C_D}{\tau_P} \frac{\mathrm{Re}_P}{24} U_{rel} \tag{22}$$

and the drag coefficient is estimated as

$$\begin{aligned} C_D &= \frac{24}{\mathrm{Re}_P}(1 + \frac{1}{6}\mathrm{Re}_P^{2/3}) \qquad \mathrm{Re}_P < 1000 \\ C_D &= 0.424 \qquad \mathrm{Re}_P \geq 1000 \end{aligned} \tag{23}$$

here X_P is the parcel position vector and U_P is the parcel velocity vector. The relative velocity U_{rel} between the parcel and the surrounding gases is denoted as $U_g - U_P$. For simplicity, the interaction between liquid and gas phases is accounted for by considering only the gravity and drag forces experienced by each parcel. The calculation of this force is given in equations (23)-(24) where the parcel Reynolds

number is expressed as $\mathrm{Re}_P = \rho_g |U_{rel}| d_P / \mu_g$ with ρ_g being the density of gas phase, d_P being the parcel diameter and μ_g being the gas phase dynamic viscosity. $\tau_P = \rho_P d_P^{\,2} / 18\mu_g$ is the time taken for a parcel to respond to local disturbances, also known as the parcel characteristic time. The instantaneous local velocity difference U_{rel} cannot be directly evaluated and requires closure. The current study employs O'Rourke's stochastic turbulence dispersion (STD) model [50] to estimate U_{rel} which, in LES formulation, can be written as

$$U_{rel} = U + U_P^{'} - U_p \tag{24}$$

where U can be obtained by solving equation (13) and $U_P^{'}$ is the stochastic velocity vector accounting for the localised dispersion of parcels through the interaction with gases. $U_P^{'}$ is assumed to satisfy a Gaussian distribution with the variance $\sigma = \sqrt{2k_{sgs} / 3}$ and the mean of zero. In this way, the Gaussian distribution $G(U_{P,i}^{'}) = 1 / \sigma\sqrt{2\pi} \exp(-U_{P,i}^{'} / 2\sigma)^2$ randomly assigns values to each component of $U_P^{'}$ at every integration step of the gas (Eulerian) phase. In each computational cell, the momentum source term in equation (14) can be then obtained from

$$\overline{S_U^s} = \frac{1}{V_{cell}} \sum \frac{d}{dt}(m_p U_{P,i}) \tag{25}$$

in which m_p is the mass of parcels under consideration and the summation is over all parcels existing in a computational cell having a volume of V_{cell}.

2.4. Secondary breakup model

According to Solsjö *et al.* [51], it is reasonable to assume that Kelvin-Helmholtz (KH) and Rayleigh-Taylor (RT) instabilities can occur simultaneously in the secondary breakup regime due to the high injection velocity. The KH-RT breakup model is therefore utilised to predict the atomisation process of secondary droplets in the LPT-LES simulation. In the present study, the KH-RT model allows the generation of parcels from the breakup of the large Lagrangian droplets (parent droplets) converted from the VOF liquid structures. Specifically, the diameters of the generated parcels (which are also referred to as child parcels) are determined by the KH-RT model after the breakup of the parent droplets. The number of fluid particles a child parcel contains is then determined by ensuring the mass conservation before and after the secondary breakup of a parent droplet. Further details of the implementation of the KH-RT breakup model as well as the model constants used in this study can be found in [35, 52].

2.5. Collision model

The collision of parcels is handled by a Stochastic Trajectory Collision (STC) model [53]. Unlike the O'Rourke collision model [54] which initiates collision of two parcels when they occupy the same computational cell and their estimated probability of collision is higher than a threshold value, the STC model takes the trajectory of each participants into account. This model considers the onset of collision between two

parcels when their trajectories intersect, and the intersection point is reached at the same time within one Eulerian integration step.

2.6. Droplet Identification Algorithm (DIA)

In this section, a parallel droplet identification algorithm developed on the basis of the original VOF method in Open-Foam is described. This algorithm is designed to identify liquid structures that are discretised by less than 5 mesh cells. At this level, the sub-grid flow physics may not be accurately predicted by LES due to the lack of a sub-grid interface tracking model. Therefore, insufficiently resolved liquid structures need to be identified for extraction after which their interaction with gas at sub-grid level can be modelled by the STD and the KH-RT secondary breakup models in the Lagrangian reference.

In the Finite Volume Method, field values such as velocity, pressure, temperature and liquid volume fraction (∂_l) are stored at the centre of the controlled volumes (mesh cells). The interpolation of the cell-centred values to the face centres based on the face flux (advection) and values in neighbouring cells is fundamental to the finite volume method. The interpolation methods and schemes are detailed in Henrik [55]. In the present study, the identification process involves grouping adjacent liquid-containing cells ($\partial_l \geq 0.05$) sharing one cell face which has a liquid volume fraction $\partial_l \geq 0.05$ to form contiguous liquid structures. The identification method is more accurate but

slower with the use of a smaller threshold liquid volume fraction and $\partial_l \geq 0.05$ is chosen by balancing accuracy and computational time. For the identified contiguous structures, velocities (U_P), centroids (x_P) and equivalent spherical diameters (R_p) are evaluated:

$$V_p = \sum_N \alpha_l V_{cell} \tag{26}$$

$$R_p = \frac{1}{2}\left(\frac{6V_P}{\pi}\right)^{\frac{1}{3}} \tag{27}$$

$$x_P = \frac{1}{V_P}\sum_N x_{cell}\alpha_l V_{cell} \tag{28}$$

$$U_P = \frac{1}{V_P}\sum_N U_l \alpha_l V_{cell} \tag{29}$$

Hereafter N is the total number of identified computational cells with a liquid volume fraction greater than 0.05. The summation is over all identified mesh cells that belong to a complete liquid structure. The identification process is shown in Figure 3.

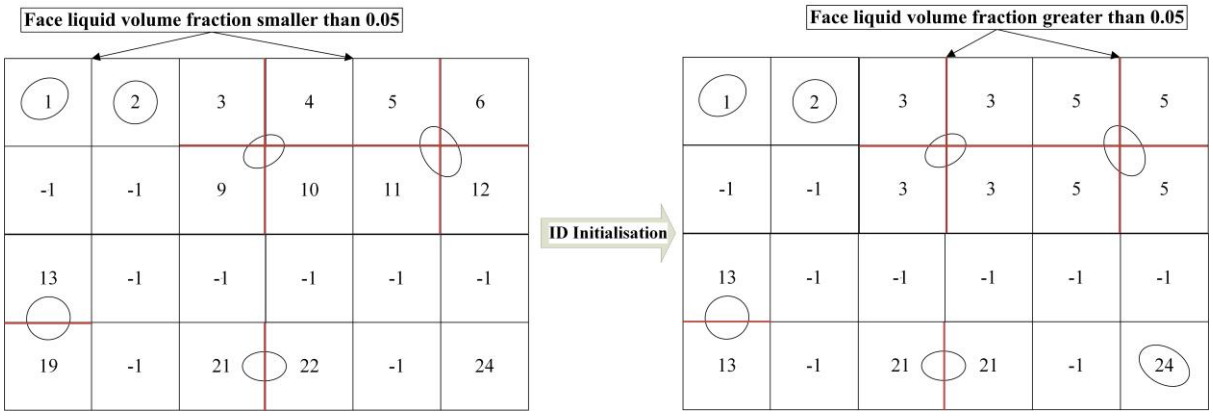

Figure 3: ID initialisation of liquid structures. Adjacent liquid-containing cells sharing a cell face with $\partial_l \geq 0.05$ (marked in red) are combined to form contiguous liquid structures. The ID of a combined liquid structure is changed to be the same as the associated cell bearing the smallest ID. An individual cell containing liquid but not having a liquid containing neighbour is also identified as an individual liquid structure. Cells of zero liquid volume fraction are tagged with -1.

To ensure the uniqueness of every liquid structure across the entire domain, the next step is to update the IDs of all liquid structures according to the rank of their host processor, as depicted in Figure 4.

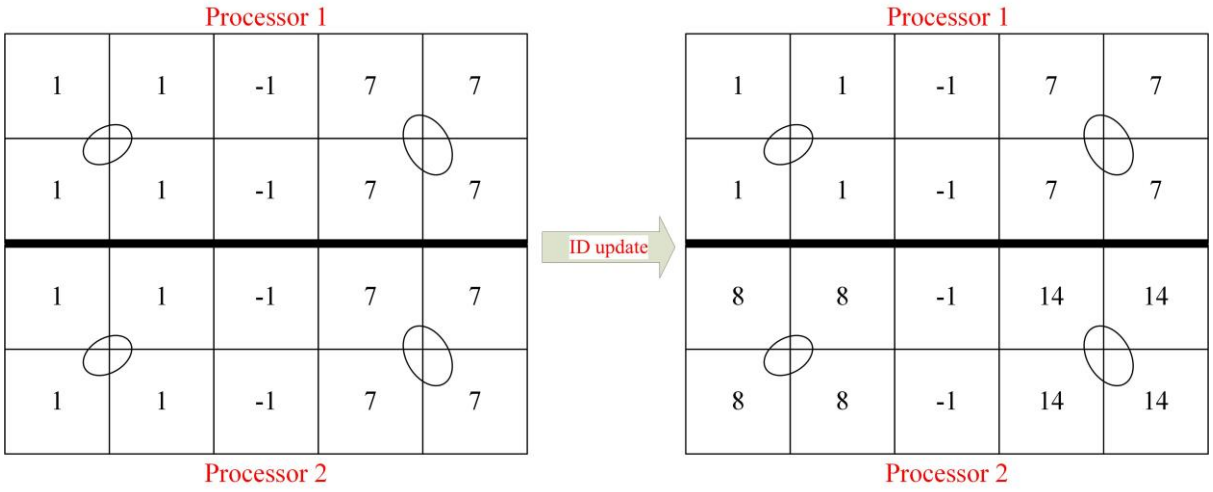

Figure 4: Updating of the liquid structure IDs across the computational domain. Each processor adds the maximum ID received from its higher ranked neighbour to its local liquid structures to ensure the uniqueness of every liquid structure in the domain.

In parallel computing mode, another important point that should be considered is the preservation of liquid structures that are on or approaching processor patches. This is because when a liquid structure moves from one processor to another, it is possible for it to be broken into droplets that are then erroneously extracted from the domain by the Droplet Extraction Algorithm (DEA). This algorithm identifies liquid structures smaller than a pre-defined volume threshold, extracts and converts them to spherical droplets (by assigning $\alpha_l = 0$ to corresponding cells in the VOF domain) that are injected into the Lagrangian domain. This situation is illustrated in Figure 5.

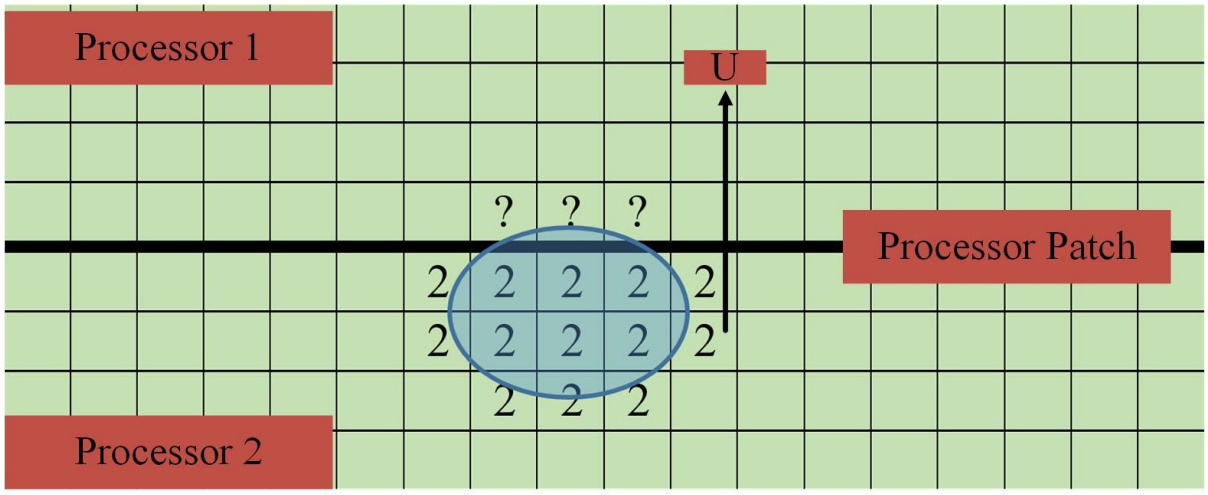

Figure 5: A liquid structure (ID=2) which is crossing the processor patch with a velocity U. The portion that could be erroneously extracted is tagged with question marks.

When a liquid structure crosses the processor patch, one cell in processor 1 will experience an increase in liquid volume fraction. Initially, as the liquid content might be too small to occupy this cell and there are no neighbours with $\alpha_l > 0$, the liquid contained would be recognised by the DEA as a suitable candidate for liquid structure-droplet conversion if a threshold of one cell volume was defined. Consequently, the entire liquid structure shown in Figure 5 would be non-physically extracted and transferred into same size Lagrangian droplets. These droplets could have a volume smaller than or equal to the volume of the first host cell in processor 1, and it largely depends on the size of computational time step that governs the rate at which volume fraction increases in this cell. The degree of this problem is increasingly noticeable when high temporal resolution is required, especially when running LES.

A protection algorithm is thus developed and implemented to tackle this problem. It simply stores IDs of all cells that are on processor patches in a Hash-table as different

keys. These "keys" are triggered to locally deactivate the DEA when a liquid structure is detected to infect processor patch cells. The DEA therefore only applies to extract small liquid structures that are not on or in close proximity to process patches.

Finally, properties of all the extracted liquid structures are sent to the master processor by its slaves and are stored in three Hash-tables (Table 1) designated to record liquid structures' (pre-LPT droplets) IDs and their corresponding x_p, U_p and R_p.

Table 1: Hash-tables storing properties of pre-LPT droplets.

Hash-table 1		*Hash-table 2*		*Hash-table 3*	
Droplet ID	R_p	*Droplet ID*	x_p	*Droplet ID*	U_p
1	R_1	*1*	(x_1, y_1, z_1)	*1*	(u_1, v_1, w_1)
2	R_2	*2*	(x_2, y_2, z_2)	*2*	(u_2, v_2, w_2)
3	R_3	*3*	(x_3, y_3, z_3)	*3*	(u_3, v_3, w_3)
….	….	….	….	….	….

The implementation of the identification algorithm has a limited influence on the parallel efficiency of the original VOF code in Open-Foam, simply because it does not

increase the communications between processors as the assembly of liquid structures is strictly restricted within each processor domain. The use of the protection algorithm eliminates the need to assemble liquid structures across processors. The complete droplet identification process is schematically shown in Figure 6.

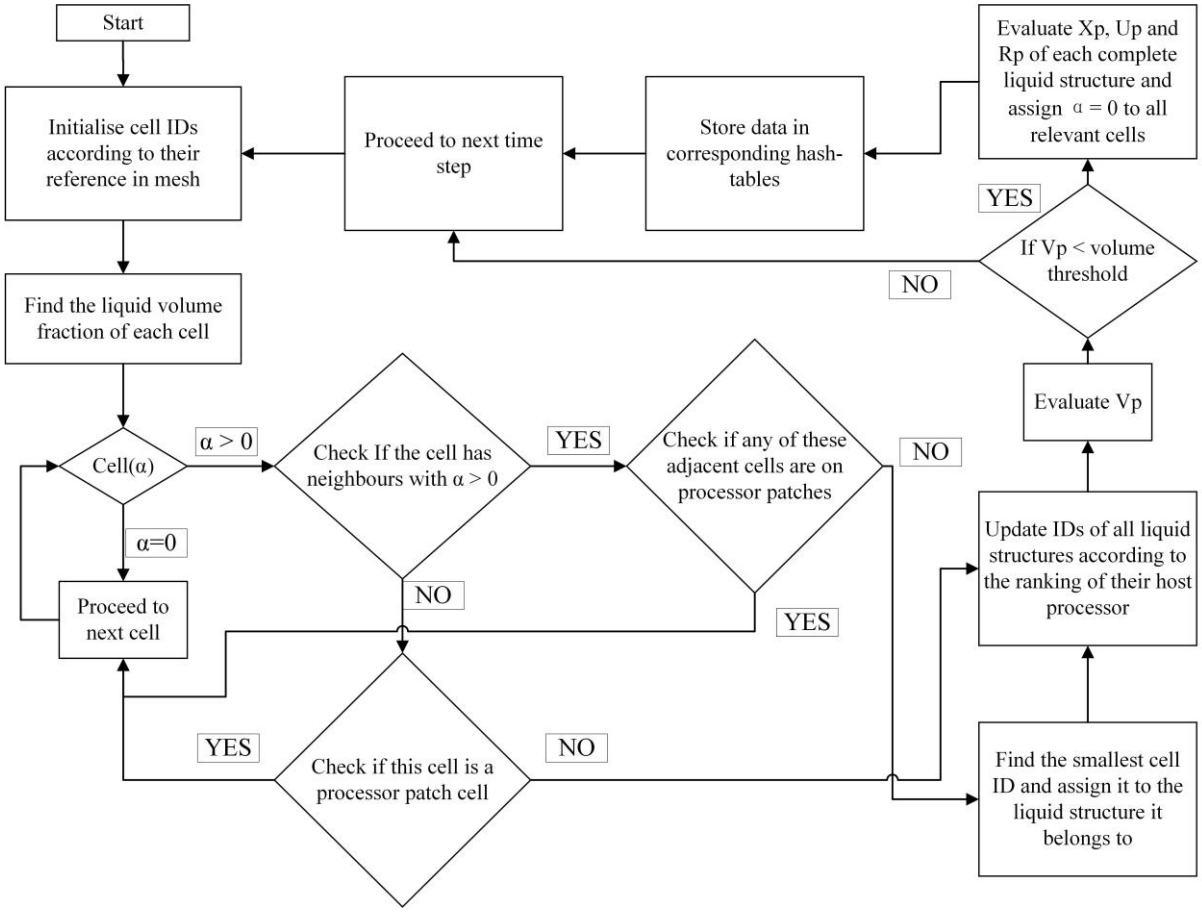

Figure 6: Flow process for parallel droplet identification algorithm.

2.7. Droplet injector

The next step in VOF-LPT coupling is the injection of droplets transferred by the DEA to the Lagrangian domain. The injection process must satisfy conservation laws in order to preserve the accuracy of coupling. This involves developing a utility able to read information from the three Hash-tables and transform them into Lagrangian droplets, preserving their mass, momentum and positions. A new automatic injector

with such capabilities is developed as part of the coupling method. This injector scans every entry in the three Hash-tables at run-time and acquires the volume, position and velocity of the droplets to be injected. The process diagram shown in Figure 7 schematically depicts how this injector works.

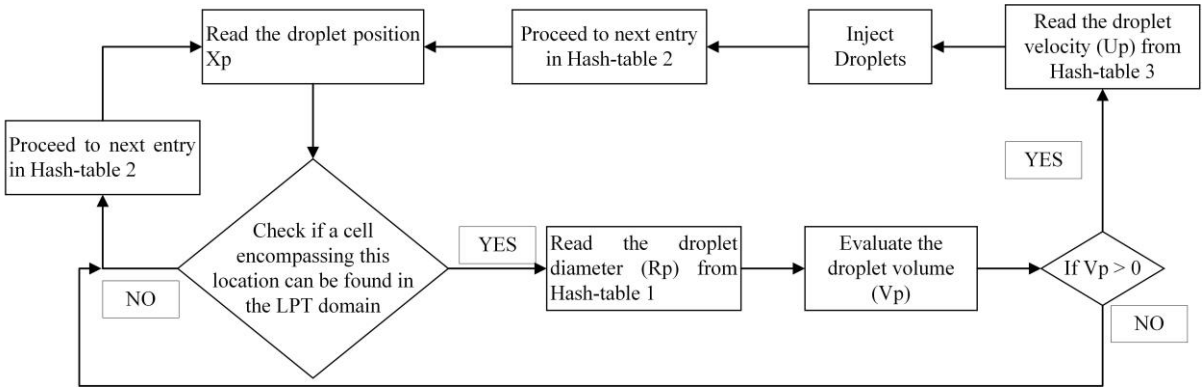

Figure 7: Process flow for the droplets injection. The customised droplet injector reads information from the Hash-tables and converts it into droplets that are injected into the LPT simulation.

3. Computational set-up

3.1. Numerical approach

Based on the recent work of Ghiji *et al.* [56], the governing equations are solved by OpenFoam using a bounded Normalised Variable (NV) Gamma differencing scheme [57] with a blending factor of 0.2 for the convection terms and an interface compression scheme (CICSAM) [58] for high resolution interface capturing. A conservative, bounded second order scheme (Gauss linear) is employed for Laplacian derivatives and a second order backward discretisation scheme is adopted for temporal terms.

3.2. Case description

This section presents a simulation of a diesel spray using the RCM. Firstly a pure VOF simulation is performed to determine the location and size of the VOF-LPT coupling region. Secondly the simulation of the diesel spray from in-nozzle flow to secondary atomisation with VOF-LPT coupling is presented. The simulation is run till only $200\,\mu s$ due to limited computing power.

Experimental conditions given in the work of Goldsworthy *et al.* [4], relevant for a non-evaporative spray from a sharp edged orifice were simulated. The n-dodecane ($C_{12}H_{16}$) was chosen as the diesel surrogate in OpenFoam. The ambient is non-reactive and initially filled with compressed air at 30bar. Boundary conditions for both simulation cases are similar to the experimental conditions in Goldsworthy *et al.* [4] and Ghiji *et al.* [48] given in Table 2. However, due to the lack of knowledge on the detailed pressure variation in the injector sac, the pressure is assumed to increase linearly from 30bar to 1200bar in $200\,\mu s$ at the sac inlet. This sac pressure ramp is similar to that used by Ghiji *et al.* [56]. More accurate modelling of the diesel spray and validation of the coupling procedure will be presented in future work.

Table 2: Experimental configurations for spray injection corresponding to the $200\,\mu s$ simulation. Nozzle diameter is used as the characteristic length.

Parameter	Value
Injection pressure	1200 bar
Nozzle diameter	0.25mm
Nozzle length	1.6mm

Nozzle index factor (K_s)	0
Fuel	Diesel
Fuel density	832 kg/m^3
Gas	Compressed air
Density ratio	42
Fuel kinematic viscosity	2.5226×10^{-6} m^2/s
Surface tension	0.03 N/m
Temperature	298 K
Chamber pressure	30 bar
Cavitation number	1.025
Fuel Reynolds number	7000≤Re≤47000

The cavitation number k is calculated from

$$k = \frac{P_{injection} - P_{vapour}}{P_{injection} - P_{ambient}} \tag{30}$$

$$\mathrm{Re} = \frac{\rho_l U_l D}{\mu_l} \tag{31}$$

3.3. Computational grid

The simulations comprise an injector and an engine chamber. The injector mesh is designed to include an inlet, a sac and a nozzle while the engine chamber mesh is shaped as a conical cylinder allowing a smooth transition of a fine grid in the nozzle to a relatively coarse grid at the end of the chamber. The geometry configuration of the computational domain is shown in Figure 8.

To achieve reasonable resolution, the smallest mesh elements of $1\,\mu m$ are distributed in the nozzle where the in-nozzle flow separation, cavitation and turbulent fluctuations

are captured. However, the cell size was not determined on the basis of the smallest turbulence scale (Kolmogorov scale) but to be sufficient for the demonstration of the operation of the transition code. The cell size is proportionally increased to $\Delta x = 0.5mm$ at the end of the chamber, with a growth rate of 1.02. The maximum cell size of 0.5mm is related to the coarsest grid used for a LPT-LES simulation of a diesel spray in Jangi *et al.* [22]. In total, 17 million hexahedral cells are used to discretise the computational domain.

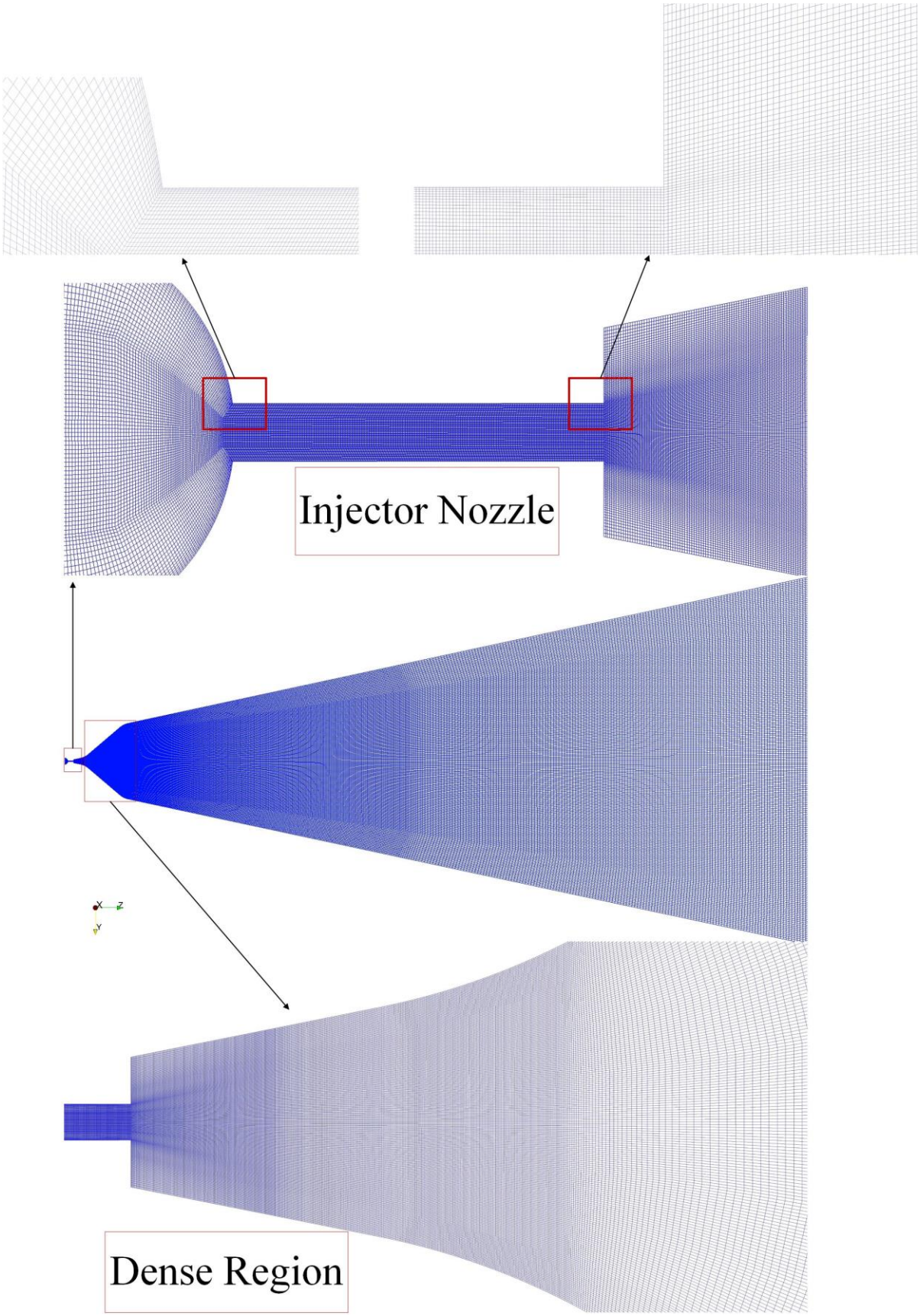

Figure 8: Computational grid design. Enlarged views are shown for the grid design in the nozzle and in the dense region where the transition from fine grid to coarse grid starts. The total number of cells are 17 million and smallest cell size is $1\,\mu m$.

The injector is initially filled with fuel up to the nozzle exit such that air is not present in the region near the nozzle entrance and the start of injection occurs shortly after the start of simulation. The VOF simulation is initiated with the boundary conditions provided in Table 3, corresponding to Figure 9. As LES is employed for turbulence modelling, the maximum Courant-Friedrichs-Lewy (CFL) number is set to 0.2, which gives an average time step size of 1.2×10^{-9}s.

Table 3: Boundary conditions for the computational grid

Boundary	Value
Sac in	Pressure inlet 30-1200 bar linearly in 200μs
Sac	No-slip and zero gradient (adiabatic)
Nozzle wall	No-slip and zero gradient (adiabatic)
Chamber in	No-slip and zero gradient (adiabatic)
Ambient	Non-reflective pressure boundary with a reference 30 bar

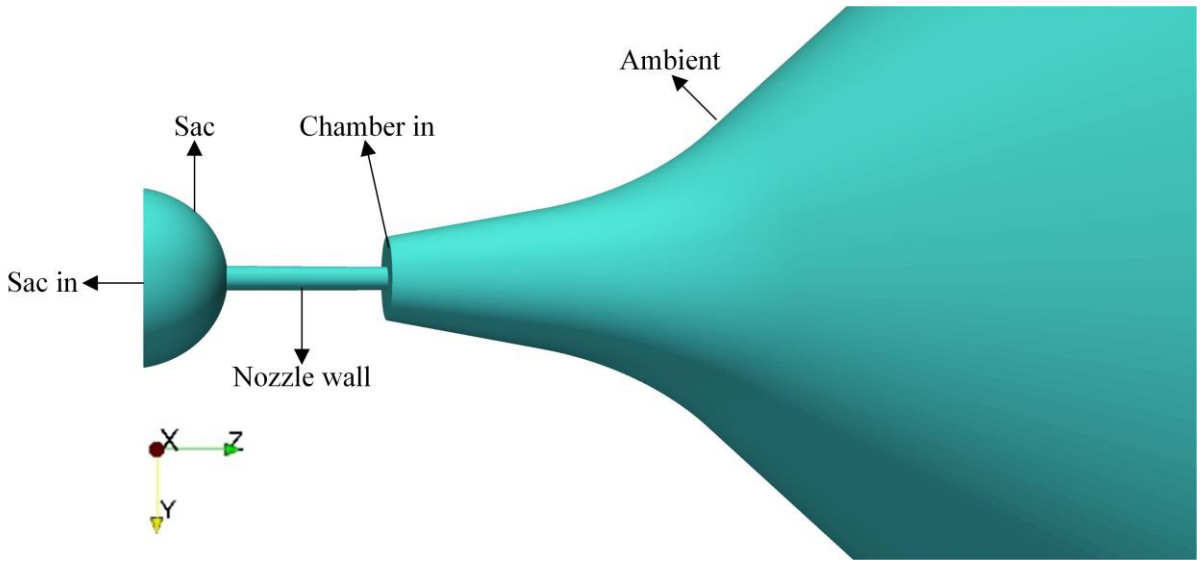

Figure 9: Boundary names and locations of the computational grid.

Due to limited computing resources, the simulation is performed on a computer cluster only using 96 core i7 (3.4GHz) processors which are granted a total of 96GB physical memory.

4. Results

4.1. Pure VOF simulation

This section presents the pure VOF simulation for determining the extent of the mesh overlap region. It demonstrates the simulated in-nozzle phenomena and primary atomisation. The volume fraction plots for the pure VOF simulation at the $x = 0$ plane for major jet breakup ($90\,\mu s$) and final ($200\,\mu s$) stages are shown in Figure 10.

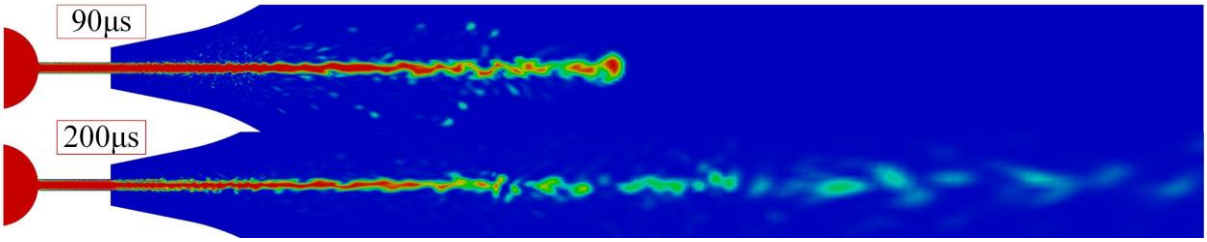

Figure 10: Fuel volume fraction shown at centre plane ($x = 0$) at 90 and $200\,\mu s$. The major jet breakup initiates at $90\,\mu s$ and the maximum extent the jet reaches at $200\,\mu s$.

Based on the pure VOF simulation, the computational domain is separated into two regions respectively for the VOF and LPT simulations. These two simulations are connected by the coupling region where the two-way mapping of velocity and pressure fields is deployed. It should be pointed out that the overlapping VOF-LPT regions have identical mesh design and elements distribution in order to ensure high fidelity field mapping between two simulations. After the grid separation, the maximum cell size in the coupling region is $\Delta x = 0.215mm$.

As shown in Figure 11, the geometry information on the injector is obtained from Ghiji *et al.* [48]. The length and the maximum diameter of the conical section of the mesh in

the chamber are based on the spray angle and spray penetrating length reported in Bong [28]. All dimensions are normalised by the nozzle diameter.

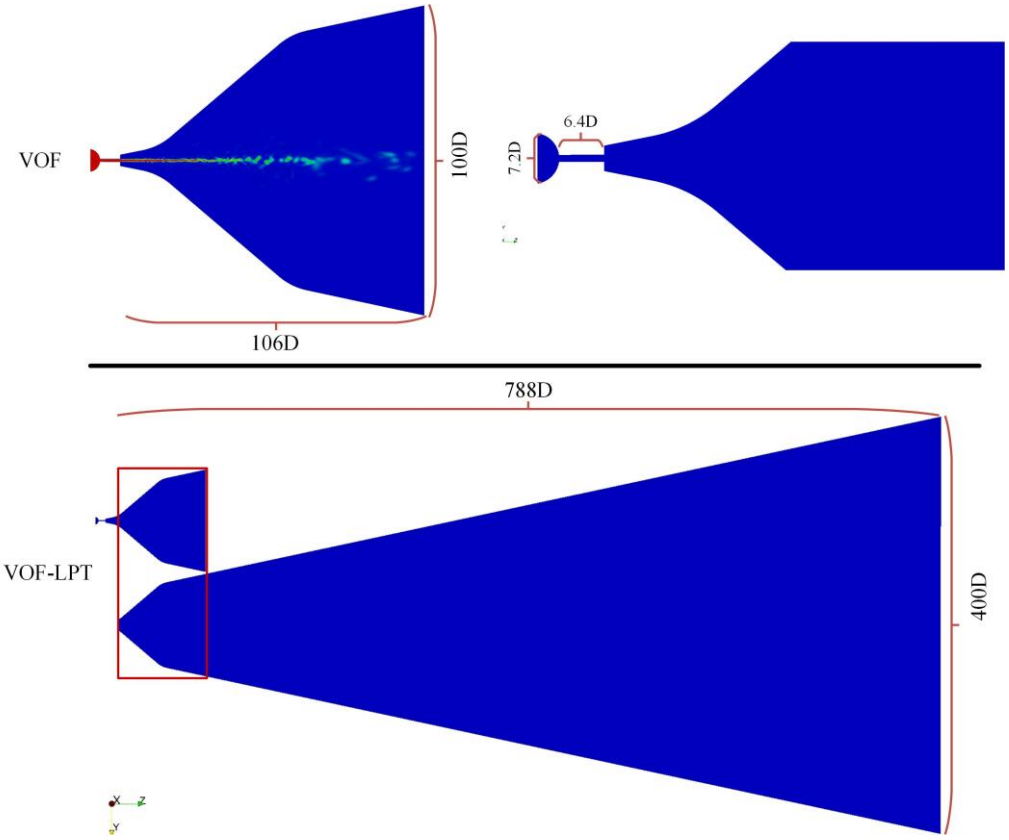

Figure 11: The geometry information for the VOF and LPT domains. The VOF domain is shown to encompass the entire liquid core at $200\mu s$. The dimensions of the injector are given in Ghiji *et al.* [48] while the size of the LPT domain is determined from the results reported in Bong [28]. The region squared in red represents the VOF-LPT coupling region. All dimensions are normalised by the nozzle diameter.

In Figure 12, the spray is represented by an Iso-surface of fuel volume fraction 0.05 on the right. The 'mushroom' like leading edge is formed due to the aerodynamic forces exerted by the compressed air ahead of the spray tip. The disintegration of this mushroom-like structure, due to shear stresses and breakup at the trailing edge of the structure, provides an initial mechanism for droplet formation. Surface breakup of the liquid jet occurs in the wake of this structure due to in-nozzle flow turbulence and the intensifying turbulent disturbances on the surface. As shown on the left of Figure 12,

in-nozzle cavitation can also occur if the local pressure drops to vapour pressure or below, as the generation of vapour can be seen in the nozzle downstream of the entrance. It should also be pointed out that the grid size used in the nozzle is not sufficient for a quasi-DNS simulation of in-nozzle flow. This leads to the spontaneous generation of excess vapour bubbles in the nozzle. A finer mesh will be used to address this problem in future work. At the later stage, the transition to hydraulic flip occurs with complete detachment of the liquid jet from the nozzle wall.

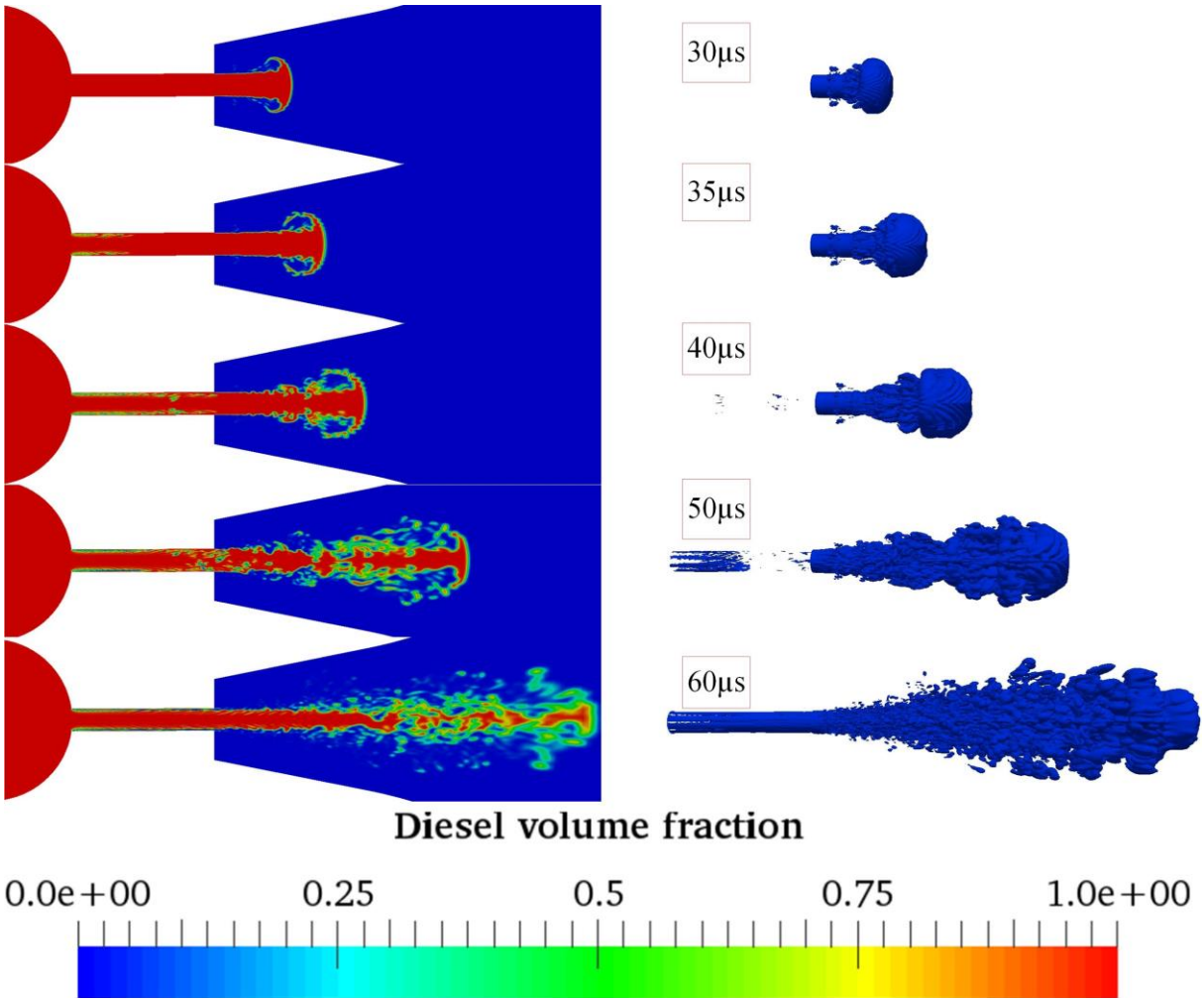

Figure 12: Diesel volume fraction plot at 30, 35, 40, 50 and 60 μs. Images on the left show the diesel volume fraction at the centre plane $(x = 0)$. The Iso-surface of the liquid jet displayed with $\alpha_l = 0.05$ is shown on the right at the same instants.

The velocity and vorticity plots in Figure 13 reveal the increase in flow velocity and the formation of in-nozzle turbulence after the sharp nozzle entrance, due to flow separation and the onset of cavitation. It can be observed that the generation of vortices is initialised when the liquid passes the sharp entrance. As the injection velocity increases, the vorticity of the flow in the nozzle and near the nozzle exit is further strengthened, causing an increase in the intensity of turbulent disturbances on the liquid surface after nozzle exit, as seen in Figure 13 from $30\mu s$ to $50\mu s$. However, it is also noticed that once the flow has separated from the nozzle entrance and transition to hydraulic flip has occurred, the turbulence intensity becomes relatively lower both in the nozzle and on the liquid jet surface as shown in Figure 13 at $60\mu s$.

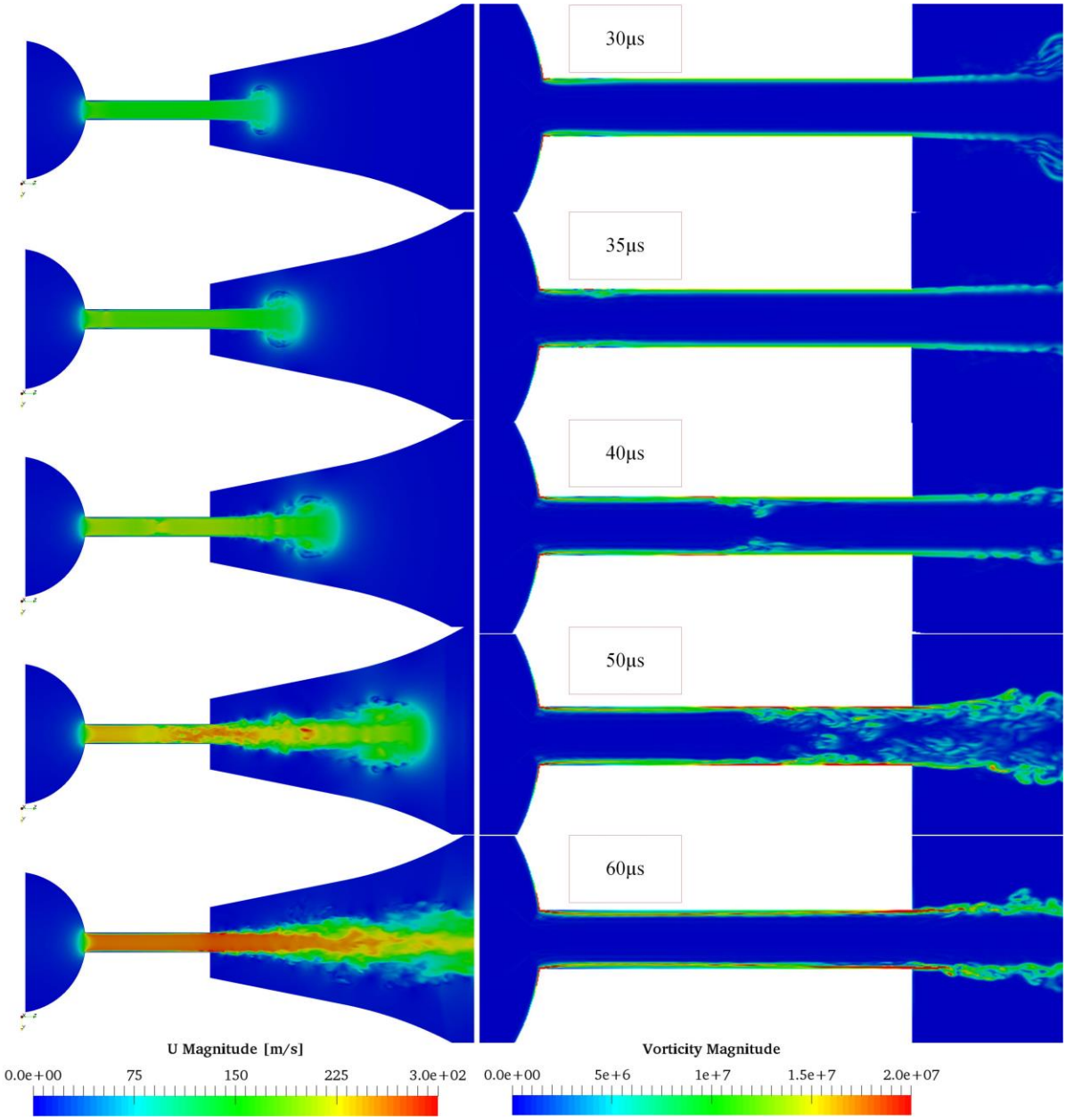

Figure 13: Contour plots of the velocity (left) and the in-nozzle vorticity (right) magnitudes at the centre plane ($x = 0$) at 30, 35, 40, 50 and 60 μs.

4.2. VOF-LPT coupling

4.2.1. Droplet identification and extraction

The demonstration of the droplet extraction and identification is performed in the first microsecond of the VOF-LPT coupling simulation, between 90us and 91us after start of injection. During this 1 us period, around 3500 liquid structures that are smaller

than 20% of their host cells are identified. The physics of these liquid structures can no longer be accurately predicted by the VOF-LES method and therefore they are extracted from the VOF domain, inserted and modelled in the LPT domain as shown in Figure 14. As shown in Figure 15, the number of VOF droplets that are discretised by less than 5 cells decreases significantly after extraction.

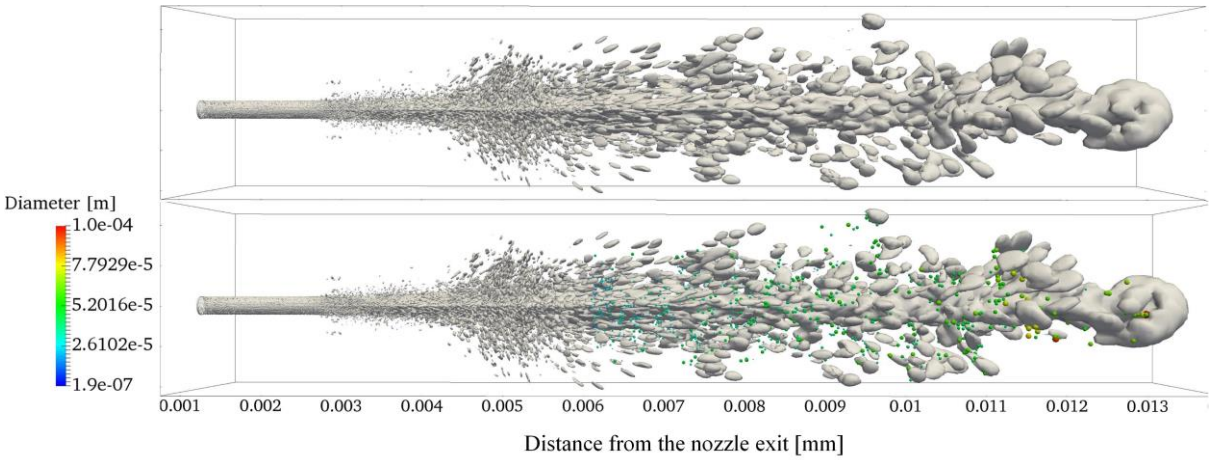

Figure 14: Displayed Iso-surface ($\alpha = 0.05$) of the liquid volume fraction coloured in grey at 90 and 91μs. The extraced droplets are converted into Lagrangian droplets which are scaled and coloured according to thier diameters.

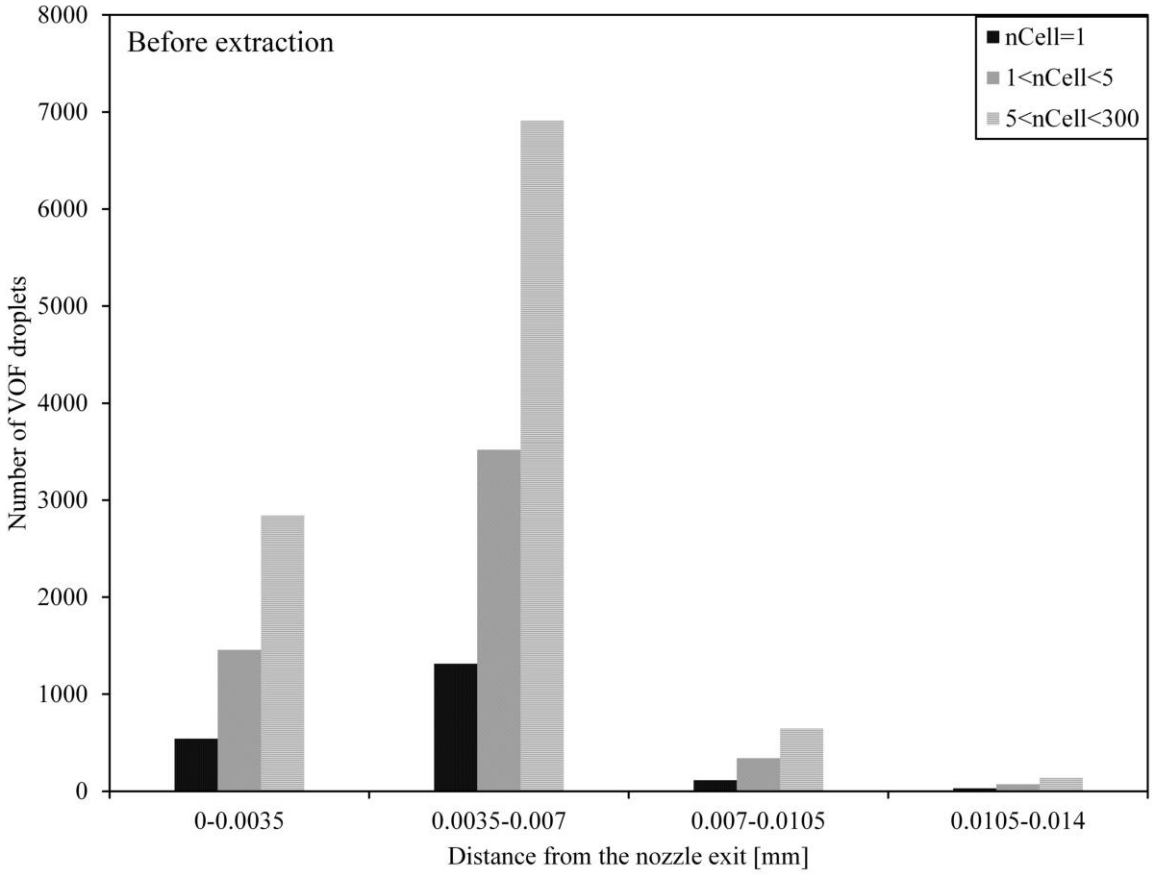
Before extraction
nCell=1
1<nCell<5
5<nCell<300
Number of VOF droplets
8000
7000
6000
5000
4000
3000
2000
1000
0
0-0.0035
0.0035-0.007
0.007-0.0105
0.0105-0.014
Distance from the nozzle exit [mm]

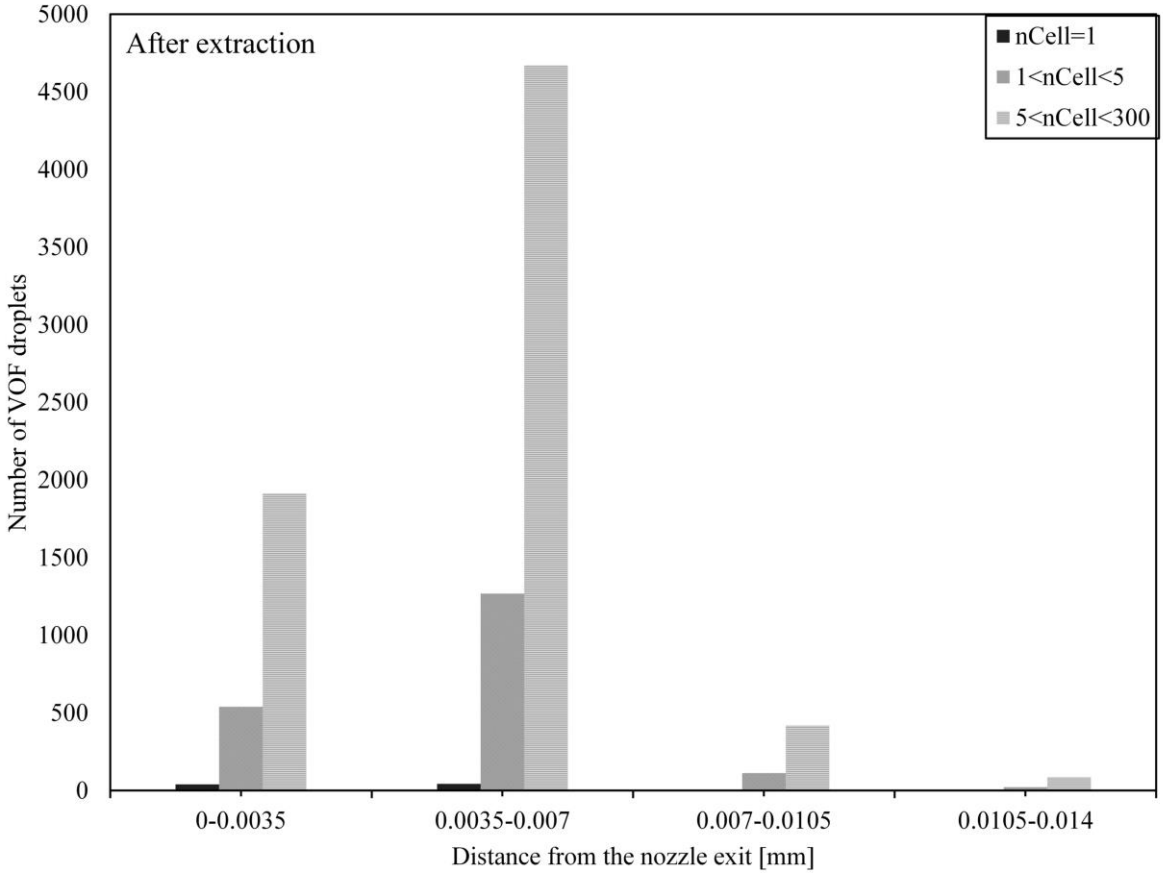
After extraction
nCell=1
1<nCell<5
5<nCell<300
Number of VOF droplets
5000
4500
4000
3500
3000
2500
2000
1500
1000
500
0
0-0.0035
0.0035-0.007
0.007-0.0105
0.0105-0.014
Distance from the nozzle exit [mm]

Figure 15: Number of VOF droplets captured by 1 mesh cell, between 1 and 5 cells and by greater than 5 cells pre- (top) and post- (bottom) extraction. After extraction, more than 90% of the droplets captured by less than 5 mesh cells are extracted and converted to Lagrangian droplets.

4.2.2. Secondary atomisation

Major spray breakup was simulated to occur from $90\,\mu s$, hence the simulation of the secondary atomisation is initiated from $90\,\mu s$ and is linked to the primary atomisation through the RCM. The two-way field coupling of pressure and velocity fields allows the effects of in-nozzle cavitation, flow separation and turbulence to be conveyed to the LPT simulation and the effects of LPT droplet-gas interaction to be reflected in the VOF simulation. The field coupling is performed at every Eulerian time-step during the VOF-LPT simulation. The field mapping results between two simulations in the overlap region at $200\,\mu s$ as can be seen in Figure 16.

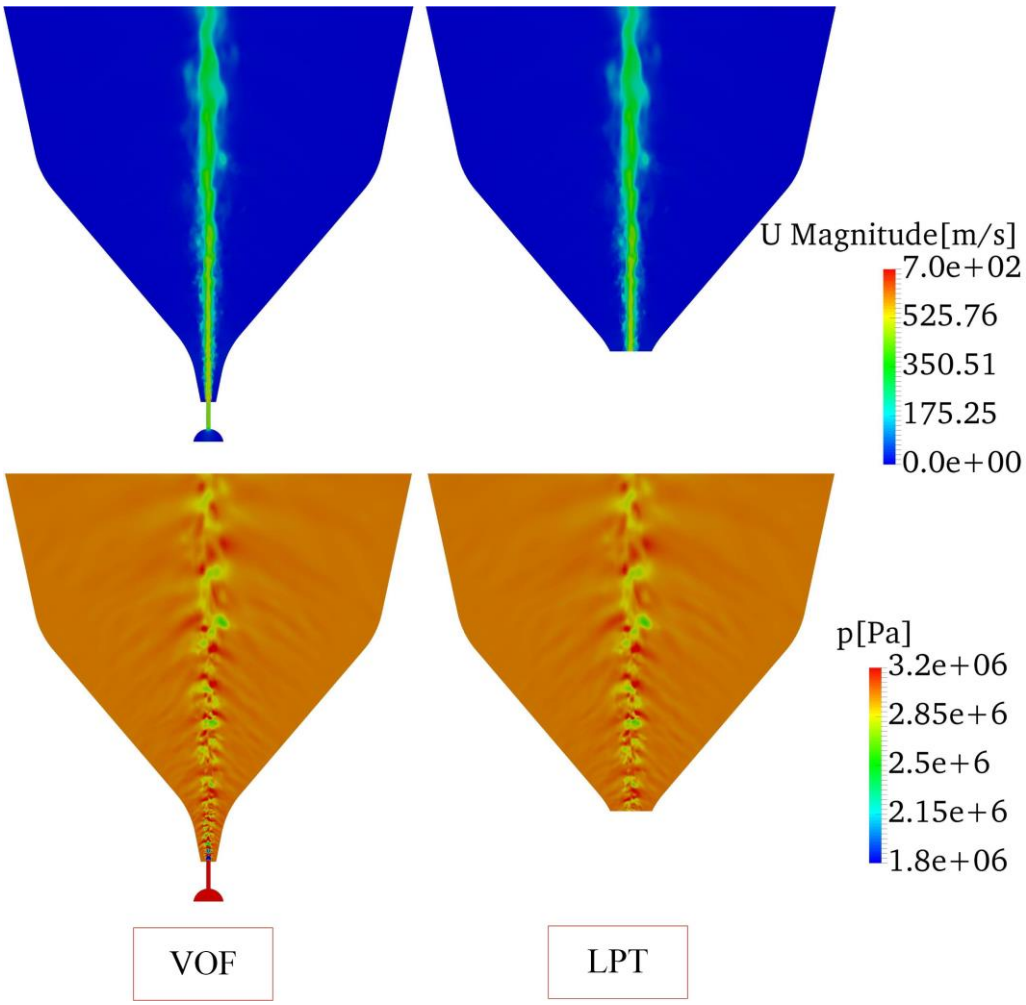

Figure 16: Mapping of velocity and pressure fields between the VOF and LPT simulations at $200\,\mu s$. The pictures on the left show contour plots of pressure at the centre plane ($x = 0$), while the pictures on the right display the velocity magnitudes at the centre plane ($x = 0$).

The field mapping between two identical grids preserves the field information in the mapping process. The high-fidelity exchange of field data between two simulations, as shown in Figure 16, enables high resolution coupling of VOF-LPT. The complete coupling procedure is illustrated in Figure 17.

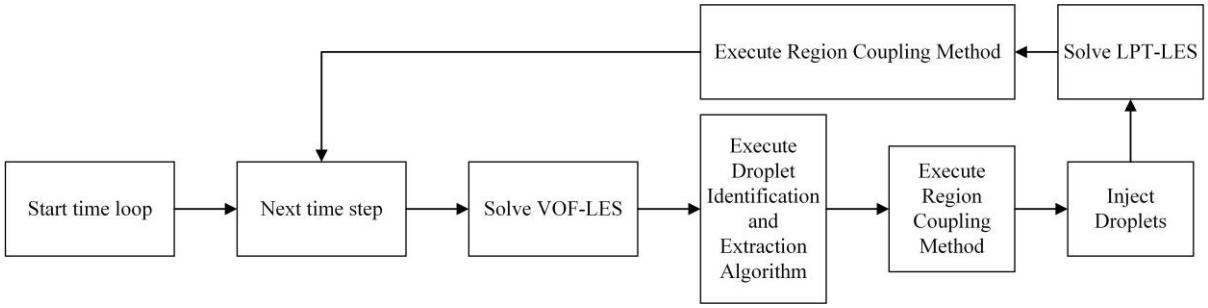

Figure 17: The complete flow process for the VOF-LES/LPT-LES coupling procedure. The complete process combines the DIA, the DEA, the droplet injection and the RCM.

The minimum and maximum cell sizes ($\Delta x_{min} = 0.02mm, \Delta x_{max} = 0.215mm$) in the coupling region give two threshold volumes of $8 \times 10^{-15} m^3$ and $1.98 \times 10^{-12} m^3 (0.2 \times \Delta x^3)$ respectively. These threshold volumes are correlated to droplets having a largest diameter of $77.9\,\mu m$. These droplets are sufficiently large to undergo secondary breakup in the LPT-LES simulation. This is modelled by the KHRT secondary breakup model, which generates child parcels containing smaller droplets of similar properties. For simplicity, the implementation of an algorithm that transfers Lagrangian droplets back into Eulerian liquid structures is not considered in the present study.

Figure 18 shows the atomised diesel jet, the transferred Lagrangian droplets, and the remaining captured phase interface geometry at 100, 125, 150, 175 and $200\,\mu s$ after start of injection. At $200\,\mu s$ after injection, approximately 54000 droplets have been transferred into Lagrangian simulation. Diameters of these transferred droplets range from the $0.3\,\mu m$ up to $70\,\mu m$, which indicates a wide spectrum of droplet diameters attributed to the RCM. These droplets undergo secondary atomisation that generates

around 64000 parcels in total. With the intensifying droplet-gas interaction, the turbulent effects of the flow on the droplets at the sub-grid level increases the spacing between droplets and produces a more dispersed spray cloud. This is mainly attributed to the implementation of the LES stochastic droplet dispersion model. The breakup of secondary droplets is statistically represented by the droplet-size distribution in Figure 19. The size distribution at four instants continuously shifts to the left, indicating that the KH-RT secondary breakup model tends to decrease the mean drop diameter by reducing the size of parent droplets and generating smaller child parcels. The co-existing parent droplets and child parcels are displayed in Figure 20. Detailed analysis of the effects of the implementation of these two models is beyond the scope of the present work and will be considered in future work.

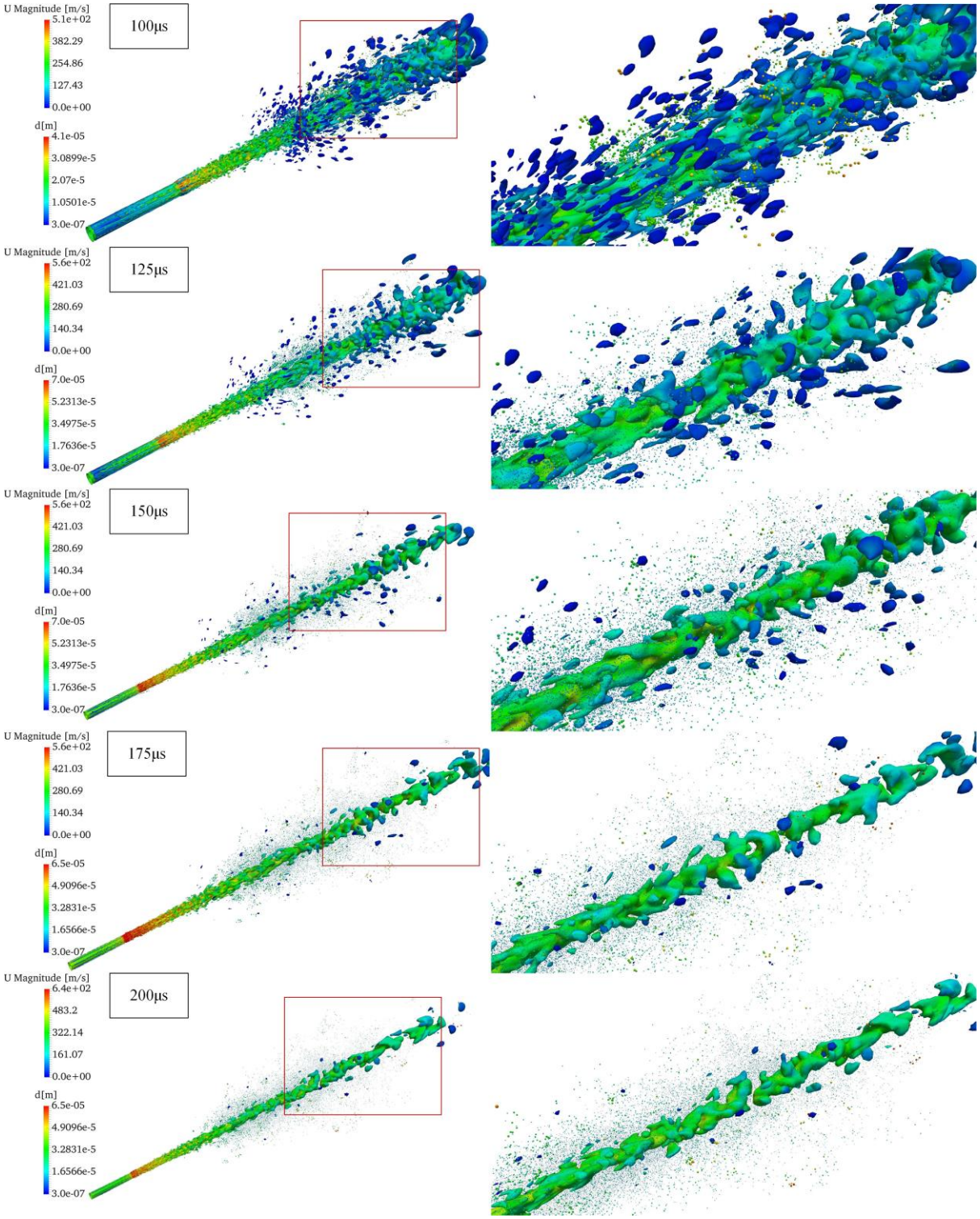

Figure 18: Secondary atomisation of the diesel fuel jet at 100, 125, 150, 175 and 200 μs after start of injection. The Iso-surface ($\alpha = 0.05$) of the liquid jet is coloured by velocity magnitude and the droplets are scaled according to their diameters. The squared area is enlarged for better clarity and is displayed on the right for all instants.

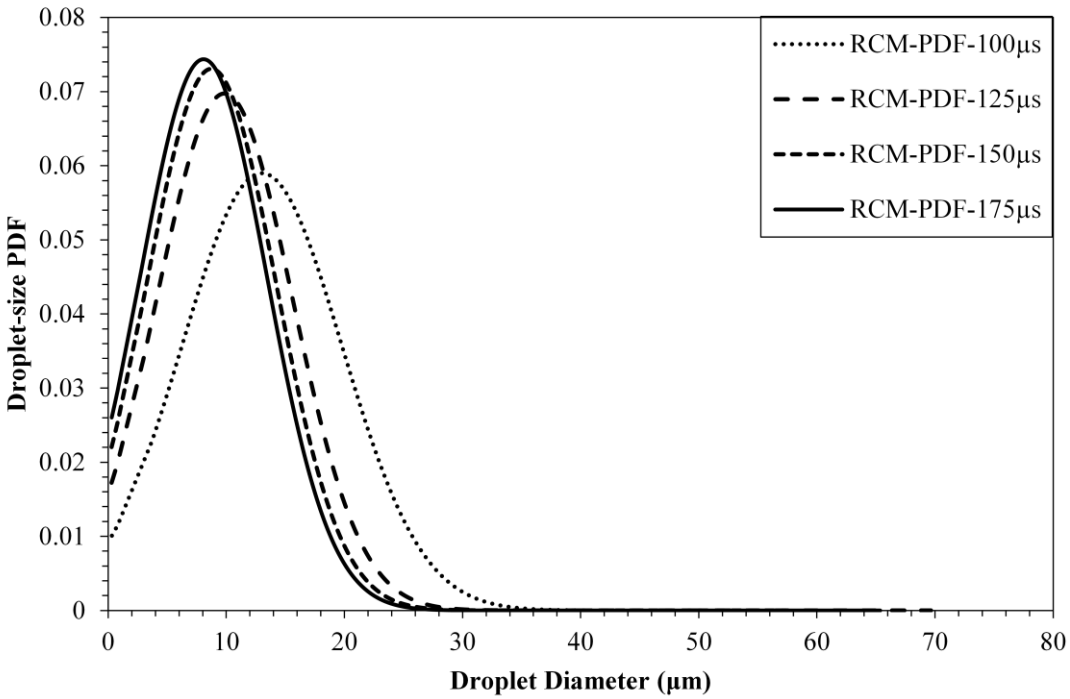

Figure 19: Comparison of Lagrangian-droplet-size distribution at five instants (t =100, 125, 150 and 175 μs after start of injection).

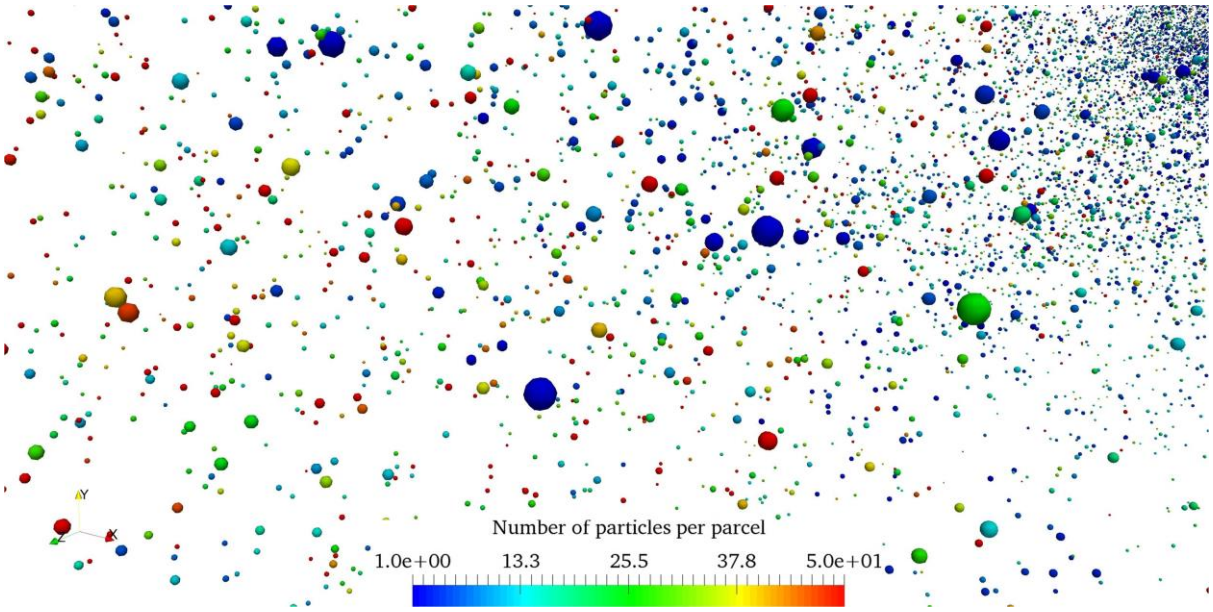

Figure 20: Large Lagrangian droplets and child parcels coloured by the number of liquid particles they contain. The large initial Lagrangian droplets are coloured in blue indicating they contain only one fluid particle before the secondary breakup. Their size decreases as they breakup into child parcels which contain a number of liquid particles. The diameter of a child parcel in the diagram is proportional to the number of liquid particles it contains.

4.3. The effect of droplet extraction on elapsed CPU time

Near the end of simulation, when the captured interface reaches its maximum extent, the total computed time needed for the DIA, DEA and RCM is continuously decreasing up to 40% from 55.505s to 33.5s (elapsed CPU time) per time-step, as shown in Figure 21. At earlier times, the required computing time is higher because the number of identified cells containing liquid in the VOF-LPT coupling region is about 35000. The speed of simulation is substantially promoted at later stages with the identified cell number reducing to around 12000 at 200μs, owing to the DEA.

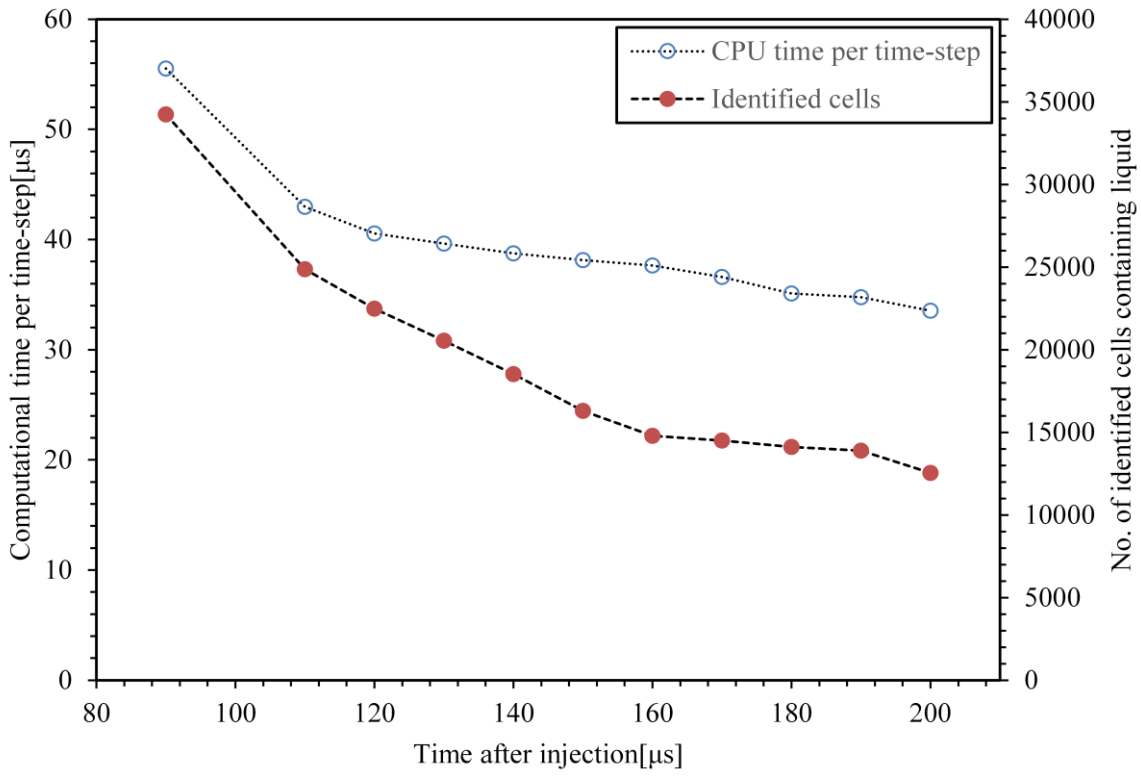

Figure 21: Observed speed up for the VOF-LPT simulation.

5. Conclusion

In this paper a parallel VOF-LES/LPT-LES coupling procedure between an Eulerian Volume of Fluid /LES and a Lagrangian Parcel Tracking/LES is presented. The

coupling procedure links the VOF and LPT simulations with the parallelised droplet identification, extraction and insertion algorithms and a region coupling method that are deployed in the VOF-LPT transition region. The use of two identical grids in the transition region enables high-resolution coupling of velocity and pressure fields between VOF-LES and LPT-LES. The implementation of the KH-RT, the LES Stochastic Turbulence Dispersion and the Stochastic Trajectory Collision models allows the use of the parcel assumption as a replacement for the point particle tracking approach in the LPT-LES simulation. The coupling procedure was applied to model a diesel spray from a sharp nozzle entrance and the capability of this procedure was demonstrated through the modelling of in-nozzle phenomena, primary and secondary atomisation.

The following characteristics of the diesel spray were modelled

- In-nozzle flow separation, cavitation and turbulence.
- The generation of turbulent disturbances on the surface of the liquid jet near the nozzle exit.
- Mushroom-like liquid structure near the nozzle exit at early injection.
- The extraction of liquid structures having a volume smaller than 20% of their host cells.
- The two-way coupling of pressure and velocity fields between VOF-LES and LPT-LES.

- The decrease in parent Lagrangian droplet size and the generation of child parcels owing to the secondary breakup regime.
- The dispersion of spray parcels due to the parcel collision and sub-grid scale turbulence.

The droplet identification, extraction and insertion algorithms together with the region coupling method were shown to be applicable to the simulation of complex diesel injection processes. The validation of the proposed coupling procedure will be considered in future work.

Acknowledgement

Significant support was received from the Australian Maritime College in terms of the access to the high performance computer clusters and installation of Open-Foam. The authors express their gratitude to Luciano Mason and Zhi Quan Leong for their support and suggestions.

References

[1] M. Gorokhovski, M. Herrmann, Modeling primary atomization, Annu. Rev. Fluid Mech., 40 (2008) 343-366.

[2] A. Fath, C. Fettes, A. Leipertz, Investigation of the diesel spray break-up close to the nozzle at different injection conditions, in: Fourth International Symposium on Diagnostics and Modeling of Combustion in Internal Combustion Engines, Kyoto, Japan, JSME, 1998, pp. 429-434.

[3] L. Goldsworthy, N. Ashraf, P. Brandner, Development of a high pressure chamber for research into diesel spray dynamics, Australian Journal of Mechanical Engineering, 7 (2009) 15-34.

[4] L. Goldsworthy, C. Bong, P. Brandner, Measurements of diesel spray dynamics and the influence of fuel viscosity using PIV and shadowgraphy, Atomization and Sprays, 21 (2011).

[5] A.L. Kastengren, F.Z. Tilocco, D.J. Duke, C.F. Powell, X. Zhang, S. Moon, Time-resolved X-ray radiography of sprays from engine combustion network spray a diesel injectors, Atomization and Sprays, 24 (2014).

[6] P. Sharma, T. Fang, Spray and atomization of a common rail fuel injector with non-circular orifices, Fuel, 153 (2015) 416-430.

[7] B. Vajda, L. Lešnik, G. Bombek, I. Biluš, Z. Žunič, L. Škerget, M. Hočevar, B. Širok, B. Kegl, The numerical simulation of biofuels spray, Fuel, 144 (2015) 71-79.

[8] Q. Xue, M. Battistoni, S. Som, S. Quan, P. Senecal, E. Pomraning, D. Schmidt, Eulerian CFD Modeling of Coupled Nozzle Flow and Spray with Validation Against X-Ray Radiography Data, SAE International Journal of Engines, 7 (2014) 1061-1072.

[9] E.d. Villiers, D. Gosman, H. Weller, DETAILED INVESTIGATION OF DIESEL SPRAY ATOMISATION USING QUASI-DIRECT CFD SIMULATION (Spray Technologies, Atomization), in: The... international symposium on diagnostics and modeling of combustion in internal combustion engines, 一般社団法人日本機械学会, 2004, pp. 295-302.

[10] C.W. Hirt, B.D. Nichols, Volume of fluid (VOF) method for the dynamics of free boundaries, Journal of computational physics, 39 (1981) 201-225.

[11] M. Herrmann, A dual scale volume-of-fluid approach for modeling turbulent phase interface dynamics, in: Proceedings of the Summer Program, 2014, pp. 69.

[12] G.M. Bianchi, P. Pelloni, S. Toninel, R. Scardovelli, A. Leboissetier, S. Zaleski, Improving the knowledge of high-speed liquid jets atomization by using quasi-direct 3d simulation, in, SAE Technical Paper, 2005.

[13] M. Sussman, P. Smereka, S. Osher, A level set approach for computing solutions to incompressible two-phase flow, Journal of Computational physics, 114 (1994) 146-159.

[14] M. Herrmann, A balanced force refined level set grid method for two-phase flows on unstructured flow solver grids, Journal of Computational Physics, 227 (2008) 2674-2706.

[15] M. Sussman, E.G. Puckett, A coupled level set and volume-of-fluid method for computing 3D and axisymmetric incompressible two-phase flows, Journal of Computational Physics, 162 (2000) 301-337.

[16] T. Ménard, S. Tanguy, A. Berlemont, Coupling level set/VOF/ghost fluid methods: Validation and application to 3D simulation of the primary break-up of a liquid jet, International Journal of Multiphase Flow, 33 (2007) 510-524.

[17] V.A. Vuorinen, H. Hillamo, O. Kaario, M. Nuutinen, M. Larmi, L. Fuchs, Effect of droplet size and atomization on spray formation: A priori study using large-eddy simulation, Flow, turbulence and combustion, 86 (2011) 533-561.

[18] B. Vreman, B.J. Geurts, N. Deen, J. Kuipers, J. Kuerten, Two-and four-way coupled Euler–Lagrangian large-eddy simulation of turbulent particle-laden channel flow, Flow, turbulence and combustion, 82 (2009) 47-71.

[19] R.D. Reitz, Modeling atomization processes in high-pressure vaporizing sprays, Atomisation Spray Technology, 3 (1987) 309-337.

[20] P.J. O'Rourke, A.A. Amsden, The TAB method for numerical calculation of spray droplet breakup, in, SAE Technical Paper, 1987.

[21] J.C. Oefelein, V. Sankaran, T.G. Drozda, Large eddy simulation of swirling particle-laden flow in a model axisymmetric combustor, Proceedings of the Combustion Institute, 31 (2007) 2291-2299.

[22] M. Jangi, R. Solsjo, B. Johansson, X.-S. Bai, On large eddy simulation of diesel spray for internal combustion engines, International Journal of Heat and Fluid Flow, 53 (2015) 68-80.

[23] S. Elghobashi, On predicting particle-laden turbulent flows, Applied Scientific Research, 52 (1994) 309-329.

[24] S. Apte, K. Mahesh, T. Lundgren, A Eulerian-Lagrangian model to simulate two-phase/particulate flows, Annual Research Briefs, (2003) 161-171.

[25] S. Apte, M. Gorokhovski, P. Moin, LES of atomizing spray with stochastic modeling of secondary breakup, International Journal of Multiphase Flow, 29 (2003) 1503-1522.

[26] R.D. Reitz, R. Diwakar, Structure of high-pressure fuel sprays, in, SAE Technical Paper, 1987.

[27] C. Baumgarten, H. Lettmann, G. Merker, Modelling of primary and secondary break-up processes in high pressure diesel sprays, in: CIMAC Congress, 2004.

[28] C.H. Bong, Numerical and experimental analysis of diesel spray dynamics including the effects of fuel viscosity, in, University of Tasmania, 2010.

[29] A. Amsden, P. O'Rourke, T. Butler, K. II, A computer program for chemically reactive flows with sprays, Los Alamos National Laboratory Rep, in, LA-11560-MS, 1989.

[30] A. Lefebvre, Atomization and sprays, CRC press, 1988.

[31] M. Herrmann, M. Gorokhovski, An outline of a LES subgrid model for liquid/gas phase interface dynamics, Proceedings of the 2008 CTR Summer Program, (2008) 171-181.

[32] W. Aniszewski, A. Bogusławski, M. Marek, A. Tyliszczak, A new approach to sub-grid surface tension for LES of two-phase flows, Journal of Computational Physics, 231 (2012) 7368-7397.

[33] M. Herrmann, A sub-grid surface dynamics model for sub-filter surface tension induced interface dynamics, Computers & Fluids, 87 (2013) 92-101.

[34] S.V. Apte, K. Mahesh, P. Moin, J.C. Oefelein, Large-eddy simulation of swirling particle-laden flows in a coaxial-jet combustor, International Journal of Multiphase Flow, 29 (2003) 1311-1331.

[35] K. Kitaguchi, S. Hatori, T. Hori, J. Senda, Optimization of breakup model using LES of diesel spray, Atomization and Sprays, 22 (2012).

[36] M. Herrmann, A parallel Eulerian interface tracking/Lagrangian point particle multi-scale coupling procedure, Journal of Computational Physics, 229 (2010) 745-759.

[37] G. Tomar, D. Fuster, S. Zaleski, S. Popinet, Multiscale simulations of primary atomization, Computers & Fluids, 39 (2010) 1864-1874.

[38] A. Burluka, R. Borghi, Development of a Eulerian model for the "atomization" of a liquid jet, Atomization and sprays, 11 (2001).

[39] A. Desportes, A combined Eulerian Lagrangian spray amortization (ELSA) in DI Diesel combustion: Fully coupled Euelrian/Lagrangian spray with ECFM-CLEH Combustion model.

[40] H. Grosshans, R.Z. Szász, L. Fuchs, Development of an efficient statistical volumes of fluid–Lagrangian particle tracking coupling method, International Journal for Numerical Methods in Fluids, 74 (2014) 898-918.

[41] B. Befrui, M. D'Onofrio, L.E. Markle, P. Spiekermann, Coupled LES Jet Primary Breakup-Lagrangian Spray Simulation of a GDi Multi-Hole Fuel Injector, SAE International Journal of Fuels and Lubricants, 8 (2015) 179-189.

[42] M.P. Musculus, K. Kattke, Entrainment waves in diesel jets, SAE International Journal of Engines, 2 (2009) 1170-1193.

[43] L.M. Pickett, J. Manin, C.L. Genzale, D.L. Siebers, M.P. Musculus, C.A. Idicheria, Relationship between diesel fuel spray vapor penetration/dispersion and local fuel mixture fraction, SAE International Journal of Engines, 4 (2011) 764-799.

[44] C. Open, OpenFOAM user guide, OpenFOAM Foundation, 2 (2011).

[45] E. De Villiers, A. Gosman, H. Weller, Large eddy simulation of primary diesel spray atomization, in, SAE Technical Paper, 2004.

[46] J. Brackbill, D.B. Kothe, C. Zemach, A continuum method for modeling surface tension, Journal of computational physics, 100 (1992) 335-354.

[47] J. Mencinger, I. Žun, A PLIC–VOF method suited for adaptive moving grids, Journal of Computational Physics, 230 (2011) 644-663.

[48] M. Ghiji, L. Goldsworthy, V. Garaniya, P. Brandner, P. Hield, CFD Modelling of Primary Atomisation of Diesel Spray, in: 19th Australasian Fluid Mechanics Conference, 2014, pp. 1-4.

[49] A. Yoshizawa, K. Horiuti, A statistically-derived subgrid-scale kinetic energy model for the large-eddy simulation of turbulent flows, Journal of the Physical Society of Japan, 54 (1985) 2834-2839.

[50] P.J. O'Rourke, Statistical properties and numerical implementation of a model for droplet dispersion in a turbulent gas, Journal of Computational Physics, 83 (1989) 345-360.

[51] R. Solsjö, X.-S. Bai, Injection of Fuel at High Pressure Conditions: LES Study, in, SAE Technical Paper, 2011.

[52] O. Kaario, V. Vuorinen, T. Hulkkonen, K. Keskinen, M. Nuutinen, M. Larmi, F.X. Tanner, Large eddy simulation of high gas density effects in fuel sprays, Atomization and Sprays, 23 (2013).

[53] P. Nordin, Complex chemistry modeling of diesel spray combustion, Chalmers University of Technology, 2001.

[54] P.J. O'Rourke, Collective drop effects on vaporizing liquid sprays, in, Los Alamos National Lab., NM (USA), 1981.

[55] H. Rusche, Computational fluid dynamics of dispersed two-phase flows at high phase fractions, in, Imperial College London (University of London), 2003.

[56] M. Ghiji, L. Goldsworthy, V. Garaniya, P. Brandner, P. Hield, Numerical and Experimental Investigation of Early Stage Diesel Sprays. Submitted for publication.

[57] H. Jasak, H. Weller, A. Gosman, High resolution NVD differencing scheme for arbitrarily unstructured meshes, International journal for numerical methods in fluids, 31 (1999) 431-449.

[58] O. Ubbink, Numerical prediction of two fluid systems with sharp interfaces, in, University of London UK, 1997.